Spatiotemporal reorganization of corticostriatal networks encodes motor skill learning

Nagham Badreddine, Gisela Zalcman, Florence Appaix, Guillaume Jean-Paul Claude Becq, Nicolas Tremblay, Frédéric Saudou, Sophie Achard, Elodie Fino

Cell Reports

Article

Spatiotemporal reorganization of corticostriatal networks encodes motor skill learning

Graphical abstract

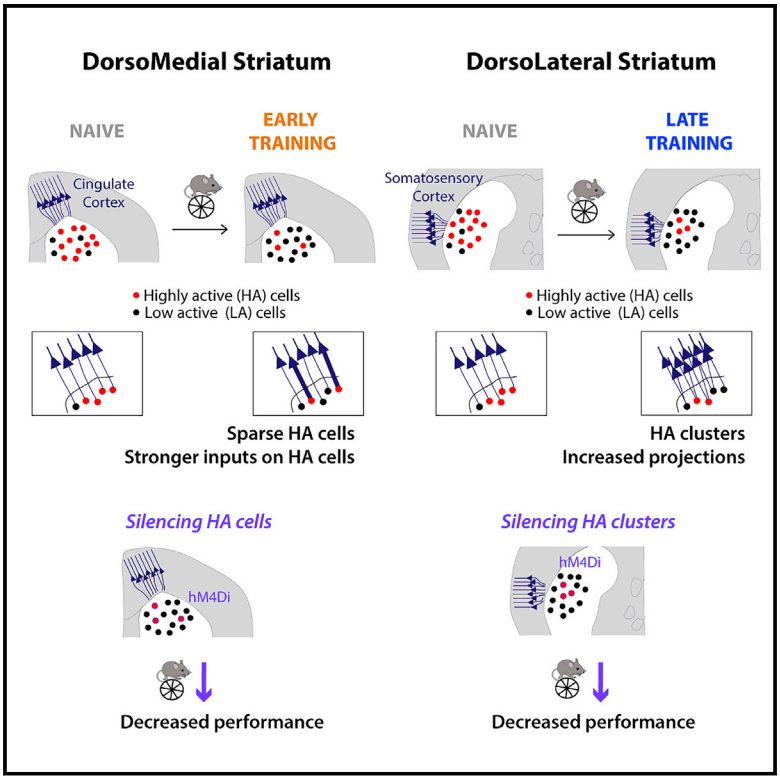

Highlights

- Motor skill learning induces specific network reorganization in the DMS and DLS
- Differently patterned highly active DMS and DLS cells are correlated with performance
- Reorganization of two territories arises from distinct levels of plasticity
- Targeted silencing of highly active cells impairs performance

Authors

Nagham Badreddine, Gisela Zalcman, Florence Appaix, ..., Frédéric Saudou, Sophie Achard, Elodie Fino

Correspondence

elodie.fino@inserm.fr

In brief

Badreddine et al. show different reorganizations of striatal activity in dorsomedial (DMS) and dorsolateral (DLS) striatum during motor learning, with the appearance of differently patterned highly active (HA) cells. These HA cells are correlated with performance and necessary for the acquisition and long-lasting retention of a motor skill.

Badreddine et al., 2022, Cell Reports *39*, 110623
April 5, 2022
https://doi.org/10.1016/j.celrep.2022.110623

CellPress

Cell Reports

CellPress
OPEN ACCESS

Article

Spatiotemporal reorganization of corticostriatal networks encodes motor skill learning

Nagham Badreddine,[1,4,7] Gisela Zalcman,[1,5,7] Florence Appaix,[1,6] Guillaume Becq,[2] Nicolas Tremblay,[2] Frédéric Saudou,[1] Sophie Achard,[3] and Elodie Fino[1,4,8,*]

[1]Université Grenoble Alpes, INSERM, U1216, CHU Grenoble Alpes, CNRS, Grenoble Institut Neurosciences, 38000 Grenoble, France
[2]Université Grenoble Alpes, CNRS, Grenoble INP, GIPSA-Lab, 38000 Grenoble, France
[3]Université Grenoble Alpes, Inria, CNRS, Grenoble INP, LJK, 38000 Grenoble, France
[4]Present address: INMED, INSERM U1249, Aix-Marseille University, 13009 Marseille, France
[5]Present address: IBBA-CONICET, Buenos Aires, Argentina
[6]Present address: Université Grenoble Alpes, INSERM U1209, CNRS UMR5309, Institute for Advanced Biosciences, 38000 Grenoble, France
[7]These authors contributed equally
[8]Lead contact
*Correspondence: elodie.fino@inserm.fr
https://doi.org/10.1016/j.celrep.2022.110623

SUMMARY

Motor skill learning requires the activity of the dorsal striatum, with a differential global implication of the dorsomedial and dorsolateral territories. We investigate here whether and how specific striatal neurons encode the acquisition and consolidation of a motor skill. Using *ex vivo* two-photon calcium imaging after rotarod training, we report that highly active (HA) striatal populations arise from distinct spatiotemporal reorganization in the dorsomedial (DMS) and dorsolateral (DLS) striatum networks and are correlated with learning performance. The DMS overall activity decreases in early training, with few and sparsely distributed HA cells, while the DLS shows a progressive and long-lasting formation of HA cell clusters. These reorganizations result from reinforcement of synaptic connections to the DMS and anatomical rearrangements to the DLS. Targeted silencing of DMS or DLS HA cells with the cFos-TRAP strategy strongly impairs individual performance. Our data reveal that discrete domains of striatal populations encode acquisition and long-lasting retention of a motor skill.

INTRODUCTION

Motor skills are the bases of a wide range of common behaviors such as riding a bicycle, driving, or playing an instrument. Mastering a new motor skill requires extensive practice leading to efficient execution, automatization, and storage of a motor command (Dayan and Cohen, 2011; Hikosaka et al., 2002). Such learning is characterized by an early phase of rapid improvement in performance followed by a late phase with moderate improvement as the motor behavior is progressively automatized and refined. Once the motor skill is learned, it is retained for a long time, suggesting that it could be stored as long-lasting changes in neural circuits (Dayan and Cohen, 2011). However, how and where these progressive changes allow formation and long-term retention of such skills is still not well understood.

Basal ganglia are key brain structures for motor learning, particularly the striatum, their main input nucleus (Doyon et al., 2009; Graybiel and Grafton, 2015; Hikosaka et al., 2002; Yin and Knowlton, 2006). Indeed, corticostriatal pathway display long-term plasticity (Di Filippo et al., 2009; Koralek et al., 2012; Lerner and Kreitzer, 2011; Rothwell et al., 2015; Yin et al., 2009) and enhanced cortical inputs (Kupferschmidt et al., 2017) that have been associated with motor learning. The striatum integrates inputs from many cortical areas, and different striatal sub-regions are defined by the existence of functional corticobasal ganglia-thalamocortical loops (Gruber and McDonald, 2012; Redgrave et al., 2011). The dorsomedial striatum (DMS) is part of the associative loop, and the dorsolateral striatum (DLS) is part of the sensorimotor loop. They both play a role during the different phases of motor learning, from early acquisition to late automatism. A preferential implication of DMS in the early phase and DLS in the late phase was first described, with evidence coming from lesions and inactivation studies targeting either the DMS or the DLS (Durieux et al., 2012; Packard and McGaugh, 1996; Yin and Knowlton, 2006; Yin et al., 2004, 2006, 2009) and later on from neural global recordings in both circuits (Costa et al., 2004; Thorn et al., 2010; Smith and Graybiel, 2013; Yin et al., 2009). Although this territory dichotomy was widely described, recent evidence showed a more intermingled activity within the two striatal circuits during motor learning (Bergstrom et al., 2018; Kupferschmidt et al., 2017; Vandaele et al., 2019).

Altogether, this evidence highlights the involvement of both striatal territories in motor learning. However, it does not offer an insight into how this learning is encoded and retained within

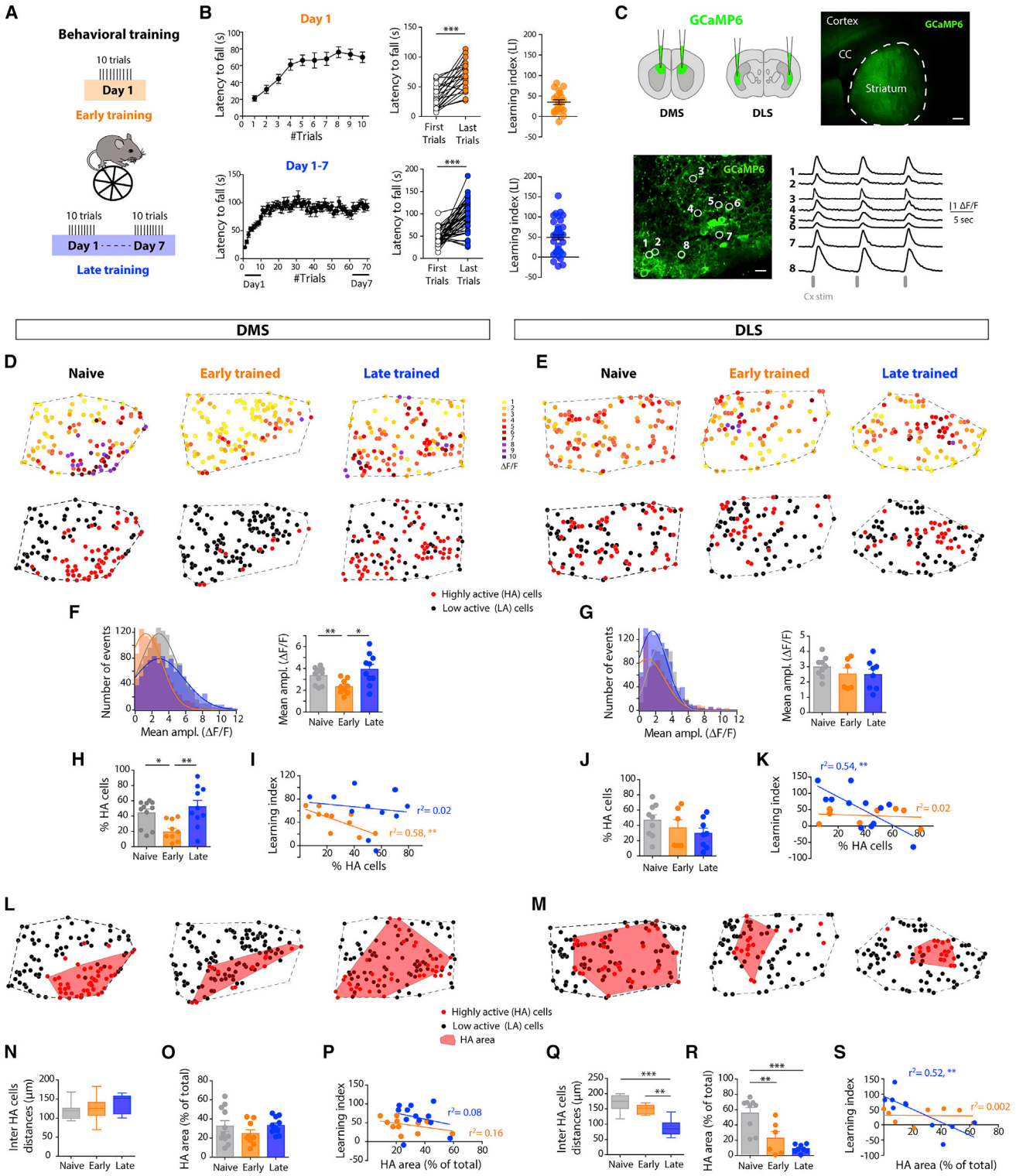

Figure 1. Motor skill learning induces a strong and specific reorganization of striatal networks

(A) Accelerating rotarod was used for early training, 10 trials in 1 day, or late training, 10 trials a day for 7 days.

(B) Significant improvement in the performance of the mice between the first and the last trials (early: mean latency to fall was 32.8 ± 4.5 s for the first trials and 67.9 ± 5.3 s for the last trials, n = 21 mice) or the first and the last day of training (late: mean latency to fall was 45.1 ± 2.7 s for first trials and 94.2 ± 5.7 s for last trials, n = 40 mice). Scatterplots show the learning index (LI) of all mice after early (averaged LI of 35.1 ± 5.6) and late training (averaged LI of 48.9 ± 6.3).

(legend continued on next page)

large populations in the two circuits. We hypothesized here that specific functional striatal populations could be responsible for the formation and consolidation of a motor skill. To identify them, we explored the changes in striatal spatiotemporal dynamics associated with learning with single-cell resolution, using *ex vivo* two-photon calcium imaging. We reasoned that recording the activity of networks with identified striatal projection neurons (SPNs) could uncover specific activity patterns directly related to motor learning. We trained mice on an accelerating rotarod and probed the network activity at different stages of learning. To disambiguate the respective involvement of DMS and DLS, we recorded the activity in both circuits. We also explored the underlying mechanisms giving rise to the activity patterns using a combination of electrophysiology, anatomical tracing, and behavior coupled to chemogenetics.

RESULTS

Specific spatiotemporal reorganization of the DMS and DLS networks during motor learning

To assess motor learning in mice, we used the accelerating rotarod task, a commonly used rodent motor learning paradigm (Buitrago et al., 2004; Cao et al., 2015; Costa et al., 2004; Kupferschmidt et al., 2017). We observed a strong and stable motor learning in mice (Figures 1A and 1B), with an improvement from the early phase (1 day) to the late phase of training (7 days). The performance of the mice was significantly increased between the first and the last trials of early training (1 day) (paired $t(20) = 6.28$, $p < 0.0001$) (Figure 1B) and further improved with late training (7 days), with a significant increase between the first and the last day (paired $t(39) = 7.66$, $p < 0.0001$) (Figure 1B). A learning index (LI) was calculated for each animal to quantify the performance (Figure 1B). To investigate the selective modifications associated with learning, we selected animals with good performance by setting the performance cutoff at the mean LI of all tested animals ($LI \geq 35$ for early training and ≥ 49 for late training).

Our aim was to explore corticostriatal network modifications associated with the different phases of motor learning. We used *ex vivo* two-photon calcium imaging in mice injected with AAV-GCaMP6f to monitor DMS and DLS SPN activity (Figure 1C), at distinct stages of motor learning (naive, early, and late phases, n = 11 naive, n = 12 early-trained, and n = 12 late-trained mice for DMS and n = 9 naive, n = 9 early-trained, and n = 11 late-trained mice for DLS; 3 early-trained mice for both DMS and DLS and 2 and 4 late-trained mice for DMS and DLS, respectively, were excluded from further analysis because they did not reach the LI criteria). We analyzed SPN activity in response to cortical stimulation in parasagittal and horizontal brain slices preserving cortical afferents to DMS and DLS, respectively (Fino et al., 2005, 2018) (Figure S1). The amplitude of responses was measured for each cell and used to build functional maps ($\approx$80–150 cells per slice) from DMS and DLS slices (Figures 1D, 1E, and S1). This would give us a picture of the network's functional organization at the different training phases.

We first measured the mean amplitude of all SPN stimulation-evoked calcium responses. In the DMS, we observed a markedly lower amplitude of SPN activity in early-trained mice ($\sim$40% decrease) (n = 956 cells, n = 9 slices, n = 9 mice) compared with naive or late-trained animals (naive, n = 1,216 cells, n = 11 slices, n = 11 mice, and late, n = 1,045 cells, n = 10 slices, n = 10 mice) ($F_{(2,27)} = 6.16$, $p = 0.006$, one-way ANOVA) (Figure 1F). Notably, despite the overall lower amplitude, a few SPNs sparsely distributed throughout the field of acquisition remained highly activated (Figure 1D). In contrast, we did not observe any change in amplitude in DLS responses ($F_{(2,20)} = 0.831$, $p = 0.4503$, one-way ANOVA; naive, n = 800 cells, n = 9 slices, n = 9 mice; early, n = 547 cells, n = 6 slices, n = 6 mice; and late, n = 749 cells, n = 8 slices, n = 8 mice) (Figure 1G).

We next analyzed the distribution of the highest activity within DMS and DLS fields. We extracted the percentage of highly active (HA) cells using the mean amplitude of responses from naive animals as a threshold to normalize the measure

(C) Schematic of the stereotaxic injections of AAV-GCaMP6f in DMS and DLS and wide-field image of GCaMP6f expression in DMS (scale bar: 200 μm). Two-photon microscopy image of SPNs expressing GCaMP6f (scale bar: 20 μm) and fluorescence traces recorded in eight DMS SPNs in response to cortical stimulation (Cx stim).

(D and E) Representative functional maps of DMS (D) and DLS (E) networks, for naive, early, and late conditions. The color code is for the amplitude of responses (ΔF/F) of active cells, with inactive cells in white. Bottom maps present the HA cells in red and LA cells in black.

(F and G) Distribution and mean amplitudes of all SPN responses in the recording field in DMS (F) and DLS (G). (F) Significant decrease of the DMS overall activity in the early condition (naive, gray, 3.3 ± 0.2, n = 11; early, orange, 2.6 ± 0.2, n = 9; and late, blue, 3.9 ± 0.4, n = 10). (G) No effect of training on DLS amplitude of responses (naive, 3.0 ± 0.2, n = 9; early, 2.5 ± 0.4, n = 6; and late, 2.5 ± 0.3, n = 8).

(H and J) Percentage of DMS (H) and DLS (J) HA cells (relative to the total number of active cells in the field) in the three conditions. DMS: percentage significantly lower in early-trained (orange, n = 9) compared with naive (grey, n = 11) and late-trained animals (blue, n = 10). DLS: percentage not significantly different in naive (n = 9 mice), early (n = 6), or late (n = 8) conditions.

(I and K) Correlation between the percentage of HA cells and the LI of the animals after early (orange) or late training (blue) in DMS (I) and DLS (K). Significant correlation for DMS early-trained mice and DLS late-trained animals.

(L and M) Maps of HA cells in red and LA cells in black after k-means analysis. Red polygons are HA area.

(N and Q) HA cell interdistance in the three conditions in DMS (N) and DLS (Q). No difference was seen in all conditions in DMS (mean interdistances were 133 ± 4 μm for naive, n = 11 mice; 135 ± 12 μm for early, n = 9 mice; and 153 ± 7 μm for late training, n = 10 mice) and a significant decrease was seen throughout the learning in DLS (mean interdistances 171 ± 9 μm for naive, n = 9 mice; 148 ± 7 μm for early, n = 6; and 89 ± 9 μm for late training, n = 8).

(O and R) Cluster area formed by HA cells: clusters of activity formed in DLS with a strong and progressive decrease in the area through learning (R). No cluster of activity in DMS (O).

(P and S) Correlation between the percentage of HA cluster area (relative to total area of the field) and the LI of the animals after early (orange) or late training (blue) in DMS (P) and DLS (S). No significant correlation, neither for early-trained mice nor for the late-trained mice condition in DMS. In DLS, there is a significant correlation only for the late-trained mice. *p < 0.05, **p < 0.01, ***p < 0.001. Data on bar graphs correspond to mean±SEM (standard error of the mean) and whisker-box plots to the median and 25th-75th percentiles (with min to max values).

throughout the training conditions. The percentage of DMS HA cells significantly decreased in early-trained animals compared with naive and late-trained mice (naive, 44.2 ± 5.2%, n = 11 mice; early, 19.5 ± 4.4%, n = 9 mice; and late, 52.3 ± 8.4%, n = 10 mice; $F_{(2,27)} = 5.7$, p = 0.009, one-way ANOVA) (Figure 1H), while the percentage of DLS HA SPNs remained constant for the different learning stages ($F_{(2,20)} = 1.3$, p = 0.295; naive, n = 9; early, n = 6; and late, n = 8 mice) (Figure 1J). Thus, there was a modulation of the amplitude and percentage of HA cells throughout training in DMS, but not in DLS. We thus asked whether the existence of HA cells was linked to the animal's performance on the rotarod. We evaluated the correlation between the percentage of HA cells and the LI of all animals (including the poor performers). We found that the percentage of HA cells was inversely correlated with the performance of the mice only during early stages of learning in DMS (early, $r^2 = 0.58$, p = 0.0062; late, $r^2 = 0.02$, p = 0.6689) (Figure 1I) and only for late stages of learning in DLS (early, $r^2 = 0.02$, p = 0.6998; late, $r^2 = 0.54$, p = 0.0063) (Figure 1K). This suggested (1) a link between HA cells and individual performance and (2) that animals with a restricted number of HA cells in DMS and DLS showed the best performance in the early and late phases, respectively, of motor skill learning.

A striking difference between the DMS and the DLS maps was the spatial organization of HA cells. In DLS, HA cells seemed to form spatially restricted clusters, as shown by the significant decrease in HA cell interdistances in the late condition ($F_{(2,20)} = 23.7$, p < 0.0001, one-way ANOVA) (Figure 1Q). Such rearrangement was not observed in DMS ($F_{(2,27)} = 1.9$, p = 0.1604, one-way ANOVA) (Figure 1N). To investigate this, using a k-means clustering analysis, we assessed whether there was a spatial clustering of activity and whether it was affected by learning. We found no difference in the size of the area encompassing HA cells (HA area) in DMS ($F_{(2,27)} = 0.15$, p = 0.1067, one-Way ANOVA) (Figure 1O) and no correlation between this area size and the LI ($r^2 = 0.16$, p = 0.2018, for early training and $r^2 = 0.03$, p = 0.5810, for late training) (Figure 1P), but confirmed with this analysis a decrease in the percentage of DMS HA cells that was correlated with the performance (Figure S2). In contrast, we found a spatial clustering of DLS HA cells with a strong decrease in the cluster areas in the late condition (cluster area in naive, 55.6% ± 7.1%, n = 9 mice; early, 22.7% ± 8.8%, n = 6 mice; late, 9.0% ± 1.8%, n = 8 mice; $F_{(2,20)} = 15.9$, p < 0.0001, one-way ANOVA) (Figure 1R). In addition, we found an inverse correlation between the cluster areas and the animal's performance after late training ($r^2 = 0.52$, p = 0.0083, for late training and $r^2 = 0.002$, p = 0.9118, for early training) (Figures 1S and S2).

Our results show that DMS reorganization after early training is marked by a strong overall inhibition of SPN activity with the persistence of sparse HA neurons, which strongly correlates with animals' early performance. In DLS, the progressive formation of HA cell clusters correlates with individual late performance.

HA cells have more stable responses after training

We next wondered whether HA cells would have developed specific properties compared with low-active cells (LA; corresponding to all other active cells). To investigate this, we tested how HA and LA cells respond to the network plasticity, i.e., how they adapt to increasing stimulation frequencies. We built SPN activity maps in response to four stimulation frequencies (5, 10, 20, and 50 Hz) and explored the differences between HA and LA cells. We measured the evolution of the percentage and identity of HA/LA cells, their amplitude of calcium response, and their correlation coefficient (Figures 2 and S3).

In naive animals, we observed a broader and higher activation with increasing frequencies. The percentage of DMS and DLS HA cells significantly increased between 5 and 20 Hz (DMS, paired t(10) = 3.32, p = 0.0089; DLS, paired t(8) = 3.09, p = 0.0141) (Figures 2A–2E), together with the amplitude of responses of both HA and LA cells (paired t(10) = 6.52, p < 0.0001, for HA cells and paired t(10) = 6.02, p = 0.0001, for LA cells in DMS and paired t(8) = 3.29, p = 0.0111, for HA cells and paired t(8) = 5.83, p = 0.0004, for LA cells in DLS) (Figures 2G and 2H). Thus, in naive animals, an adaptive mechanism occurs, leading to progressively stronger and broader activation of the two networks with increasing frequencies.

In trained animals, the responses of HA cells were much more stable. The percentage of DMS HA cells remained stable between 5 and 20 Hz only for early trained mice (paired t(8) = 1.04, p = 0.3318) (significant increase in late-trained animals [paired t(9) = 4.36, p = 0.0024], as in naive) (Figures 2A and 2C). Similarly, the percentage of DLS HA cells was stable across stimulation frequencies after training (early, paired t(5) = 0.37, p = 0.7251; late, paired t(7) = 1.71, p = 0.1302) (Figures 2B and 2E). This stability is represented by the similarity of the activity maps at 5 and 20 Hz for early DMS slices (Figure 2A) and late DLS slices (Figure 2B). Not only did the percentage of HA cells remain stable, but the identity of HA cells did not change across stimulation frequencies (i.e., no or few exchanges between the HA and the LA pools) (Figures 2D–2F). Regarding the amplitude of response, DMS SPN activity increased between 5 and 20 Hz in trained mice (p < 0.01 for both early and late), with a greater increase in LA cells, in contrast to naive animals, which showed no difference (Figure 2G). In DLS, the amplitude of response of HA cells was stable between 5 and 20 Hz, while it still increased in LA cells (p = 0.0039 for naive, p = 0.0313 for early, and p = 0.0078 for late) (Figure 2H). This indicated that HA cells respond similarly to increasing cortical inputs, while LA cells have the same evolution as naive animals. Finally, we also observed that both DMS and DLS HA cells had a higher correlation coefficient compared with LA cells (Figure S3).

Altogether, HA cells have more stable and correlated responses, which would lead to a more efficient transmission of cortical information.

Long-lasting reorganization in the DLS

We next asked whether late training was associated with long-lasting retention of motor skill and, more importantly, with long-lasting network reorganization. To test this, we trained animals for 7 days (day 7 versus day 1, p < 0.001, one-way ANOVA) and we evaluated the animal's motor skills 1–2 months after the first training (pre-trained group). We found that pre-trained animals performed well 1–2 months later, as shown by a higher level of performance on the first day of resumed training (pre-trained,

CellPress
OPEN ACCESS

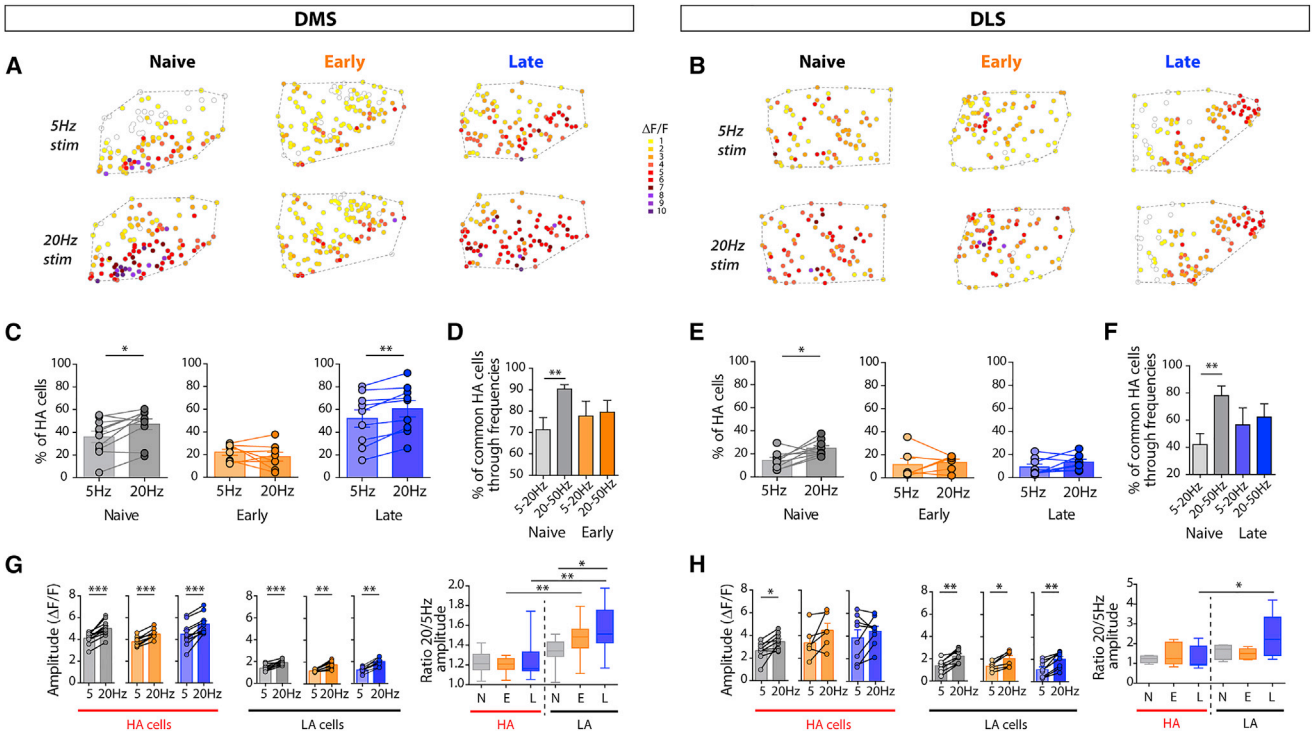

Figure 2. HA cells display more stable responses after training

(A and B) Representative maps of DMS (A) and DLS (B) network activity in response to 5 or 20 Hz trains of cortical stimulation.

(C and E) Paired percentage of HA cells in DMS (C) and DLS (E) at 5 and 20 Hz stimulation. In DMS, HA cell percentage was significantly increased in naive and late animals and remained stable in early-trained animals. In DLS, there was a significant increase in naive animals with no difference in early and late-trained animals.

(D and F) Bar graph of the percentage of common HA cells through the stimulation frequencies in DMS (D) and DLS (F). In naive animals, there was a significant increase between low and high frequencies in the number of common DMS HA cells ($p = 0.0067$, t test) and DLS HA cells ($p = 0.0046$, t test). The percentage was constant after early training in DMS ($p = 0.8421$, t test) and late training in DLS ($p = 0.7331$, t test).

(G and H) Amplitude of DMS (G) and DLS (H) response for HA (red) versus LA cells (black) for 5 and 20 Hz stimulation trains. Right, plot of the ratio 20/5 Hz amplitude for HA and LA cells. (G) Significant increase in the amplitude between 5 and 20 Hz for all the conditions (HA, $p < 0.0001$ for naive, $p < 0.0001$ for early, and $p = 0.0001$ for late training; LA, $p = 0.001$ for naive, $p = 0.0039$ for early, and $p = 0.002$ for late). There was no significant difference between HA and LA cell amplitude ratio for naive animals. The ratio was significantly higher after early and late training ($p < 0.0001$, one-way ANOVA). (H) The amplitude of DLS HA cells was significantly increased between 5 and 20 Hz only in naive. There was a significant increase for all conditions for LA cells. The amplitude ratio was significantly higher between HA and LA cells only after late training. *$p < 0.05$, **$p < 0.01$, ***$p < 0.001$. Data on bar graphs correspond to mean ± SEM and whisker-box plots to the median and 25th–75th percentiles (with min to max values).

$p = 0.0046$ between day 1 and day 1′, n = 5 mice), and had a similar maximal performance level 7 days of training later ($p = 0.6914$ between day 7 and day 7′) (Figure 3A). In contrast, the learning curve of age-matched animals that did not receive a first training session (pre-naive) was significantly lower ($F_{(1,36)} = 21.42$, $p = 0.0006$, n = 5 mice for each group, two-way ANOVA) (Figure 3A). These experiments therefore suggested that learned motor skills were preserved for months.

To confirm that HA clusters were associated with better performance in pre-trained animals, we explored the DLS network dynamics 1–2 months after the first training session (at day 1′) (Figure 3B). The amplitude of SPN responses was not significantly different between the two groups (pre-naive, 1.9 ± 0.1, n = 11 slices, n = 6 mice; pre-trained, 2.3 ± 0.2, n = 7 slices, n = 6 mice; $t(16) = 1.683$, $p = 0.1118$). However, we observed a significant reduction in the HA area in the DLS of pre-trained animals (pre-naive, 44.3 ± 6.0%; pre-trained, 19.7 ± 5.7%; $t(14) = 2.9$, $p = 0.0116$). These results showed that the long-lasting spatial reorganization of network activity in the DLS is associated with the maintenance of learned skills.

DMS HA cells display specific cortical input integration properties

What are the mechanisms responsible for DMS and DLS reorganization? We first hypothesized that they may emerge from modifications of SPNs' intrinsic electrophysiological or integration properties of cortical inputs. We thus compared the properties of HA and LA cells. We trained the animals and performed two-photon calcium imaging. We used an online analysis protocol to identify cells during image acquisitions and immediately perform targeted patch-clamp recordings of HA and LA cells in DMS of early-trained mice or in DLS of late-trained mice networks (Figure 4A).

In the DMS, no significant difference was observed in the intrinsic electrophysiological properties of HA and LA cells after early training (Figure 4B). We compared the cortical input

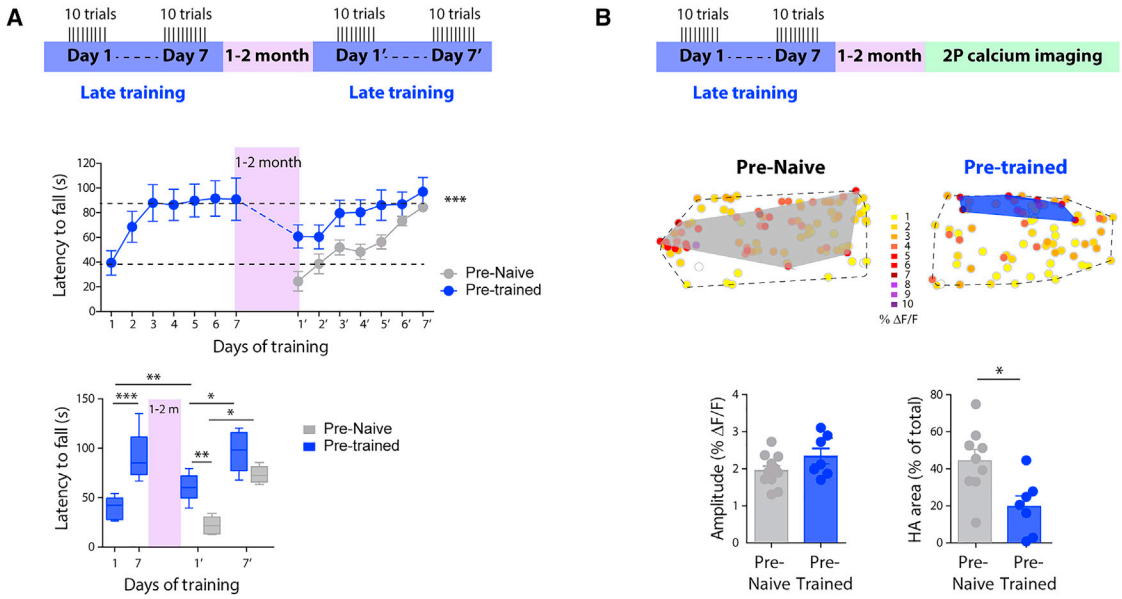

Figure 3. Long-lasting learning and associated DLS reorganization

(A) Pre-trained animals (blue) followed a first late training session and, after a gap of 1–2 months, another session (n = 5 mice). The pre-naive animals (n = 5 mice) were age matched and trained only once. After the gap, pre-trained animals' performance was higher than at the beginning of the first training and had a significantly different learning curve compared with the pre-naive animals (gray). A box-and-whisker plot of latency to fall all along the tests in the two groups is shown.

(B) Two-photon calcium imaging in pre-trained animals, 1–2 months after the first late training, and in pre-naive mice. Representative activity maps of a pre-naive and a pre-trained animal are shown. Bar graphs are of the mean amplitude of response and the HA area in the DLS in pre-naive (n = 11) and pre-trained (n = 7) animals. No significant difference in mean amplitude of response between the two groups (pre-naive, 1.9 ± 0.1, n = 11; pre-trained, 2.3 ± 0.2, n = 7) is seen. There was a significantly smaller HA area in pre-trained (19.7 ± 5.7%) compared with pre-naive (44.3 ± 6.0%) mice. *p < 0.05, **p < 0.01, ***p < 0.001. Data on bar graphs correspond to mean ± SEM and whisker-box plots to the median and 25th–75th percentiles (with min to max values).

integration properties by measuring the dynamics of supra- and sub-threshold activity evoked in SPNs by stimulations of the layer 5 cingulate cortex. HA cells combined a higher spiking probability ($t(10) = 3.747$, $p = 0.0038$, n = 6 HA/LA cell pairs) and a shorter latency to spike ($t(12) = 2.80$, $p = 0.016$, n = 7 pairs) compared with LA cells (Figure 4C), suggesting that they were more efficiently recruited by cortical afferents. Indeed, the input/output curve showed that the amplitude of excitatory post-synaptic potentials (EPSPs) was significantly stronger in HA cells across stimulation intensities ($t(12) = 2.54$, $p = 0.0258$, n = 7 pairs) (Figure 4D). We next evaluated the short-term plasticity of corticostriatal connections. The amplitude of EPSPs evoked in LA cells increased during a train of stimulations (for five stimulations at 20 Hz, $F_{(1,50)} = 12.12$, $p = 0.0048$, and for all frequencies, $F_{(1,40)} = 13.90$, $p = 0.0033$; n = 7 pairs; two-way ANOVA) (Figure 4E), as we previously reported in naive animals (Fino et al., 2018). Interestingly, the amplitude of EPSPs evoked within a train was stable in HA cells (Figure 4E), suggesting that the probability of release of cortical inputs to the DMS might be enhanced specifically on connections targeting HA cells. Altogether, DMS HA cells seemed to receive stronger inputs from cingulate cortex compared with LA cells.

In the DLS, HA and LA cells had similar intrinsic properties (Figure 4F) and did not show any difference in somatosensory cortical input integration properties. There was no significant difference in spiking probability ($t(8) = 0$, $p = 1.0$, n = 6 pairs), latency to spike ($t(8) = 0.61$, $p = 0.56$) (Figure 4G), or input/output EPSP amplitudes ($t(7) = 0.81$, $p = 0.4475$, n = 8 pairs) (Figure 4H). The short-term plasticity was also not different between HA and LA cells (for 20 Hz, $F_{(1,69)} = 0.00$, $p = 0.9611$, and for all frequencies, $F_{(1,56)} = 1.05$, $p = 0.3537$, two-way ANOVA, n = 8 HA/LA pairs) (Figure 4I) and was similar to that of naive animals (Fino et al., 2018). These results showed that in the DLS there was no difference in synaptic inputs from the somatosensory cortex to HA and LA cells.

These data demonstrate a selective synaptic plasticity of cingulate projections to DMS HA cells, while somatosensory projections to DLS HA cells seemed unaffected.

Late DLS reorganization is associated with anatomical remodeling of cortical projections

We next asked whether anatomical rearrangements could occur after motor learning. Tracing experiments using the retrograde tracer cholera toxin B (CTB) (Mandelbaum et al., 2019; Melzer et al., 2017) were performed. CTB-A_{488} was injected into the DLS (n = 5 naive, n = 4 early-trained, and n = 4 late-trained mice) and CTB-A_{555} into the DMS (n = 4 naive, n = 5 early-trained, and n = 5 late-trained trained mice) (Figure 5A). CTB was captured by cortical terminals in the striatum and retrogradely transported to cortical cell soma (Figures 5B–5F). For normalization purposes, the sum of the injection area was measured in DMS and DLS in each animal to express the number of labeled

CellPress
OPEN ACCESS

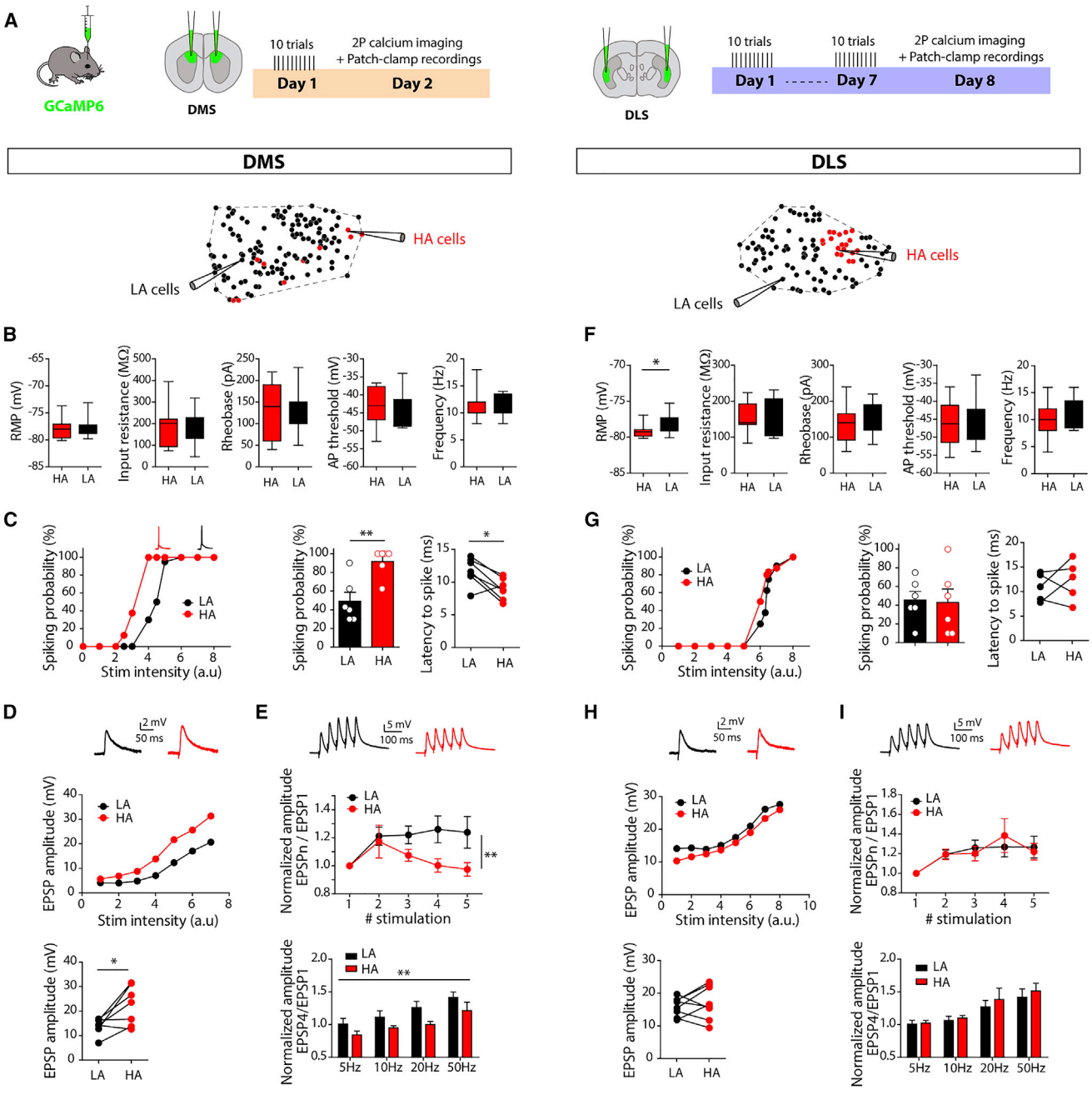

Figure 4. DMS HA cells have specific cortical input integration properties

(A) Experimental design: mice were injected with AAV-GCaMP6f and followed early (for DMS) or late (for DLS) training. Two-photon calcium imaging was performed, and live HA (red) and LA (black) cells were identified and targeted for patch-clamp recordings.

(B and F) Intrinsic electrophysiological properties of SPNs from DMS (B) and DLS (F) for HA (red) or LA (black) cells. (B) No significant difference in resting membrane potential (RMP) (HA, −77.9 ± 0.6 mV, n = 11; LA, −77.8 ± 0.5 mV; n = 12, p = 0.8068), input resistance (Ri) (HA, 190.3 ± 27.9 MΩ; LA, 175.5 ± 20.8 MΩ; p = 0.6754), rheobase (HA, 135.5 ± 19.9 pA; LA, 131.7 ± 15.5 pA; p = 0.8809), AP threshold (HA, −43.3 ± 1.7 mV; LA, −44.2 ± 1.3 mV; p = 0.6686), or frequency (HA, 10.9 ± 0.8 Hz; LA, 11.7 ± 0.5 Hz; p = 0.4439). (F) No significant difference in Ri (HA, 157.2 ± 12.6 MΩ, n = 11; LA, 155.6 ± 18.8 MΩ, n = 8; p = 0.9396), rheobase (HA, 136.0 ± 17.1 pA; LA, 148.6 ± 15.3 pA; p = 0.6108), frequency (HA, 10.2 ± 1.1 Hz; LA, 11.3 ± 1.0 Hz; p = 0.4884), or AP threshold (HA, −46.3 ± 2.0 mV; LA, −46.9 ± 2.7 mV; p = 0.8487). There was a significant difference for RMP (HA, −79.2 ± 0.3 mV, n = 11; LA, −77.9 ± 0.5 mV; n = 8, p = 0.0282).

(C and G) Representative curves of the spiking probability for HA and LA cells and quantification of spiking probability and latency to spike in DMS (C) and DLS (G). In DMS, significantly higher spiking probability and shorter latency to spike in HA cells were seen. In DLS, there was no significant difference between HA and LA cells.

(legend continued on next page)

cortical cells in cingulate (DMS) or somatosensory (DLS) cortex as a function of their targeted striatal area (Figure S4). First, for the projections from cingulate cortex to DMS, we did not observe any difference between naive and trained animals, regardless of the layer position of projecting cortical cells ($F_{2,117}$ = 1.67, p = 0.1173, two-way ANOVA) (Figure 5C). The density of CTB-A_{555}^+ cells in layer 2/3 cingulate cortex (number of cells/mm^2, normalized for injection site) was 7,000 ± 715 in naive, 9,501 ± 1,024 in early-trained, and 7,828 ± 1,474 in late-trained mice, and the number of CTB-A_{555}^+ cells in layer 5 cingulate cortex was 2,687 ± 442 in naive, 3,443 ± 335 in early-trained, and 2,171 ± 399 in late-trained mice. Thus, the cingulate cortex did not display any anatomical rearrangements induced by training. In contrast, the density of cortical somatosensory cells projecting to DLS increased in trained mice compared with naïve, with a significant increase in cortical cell density after late training ($F_{2,108}$ = 7.00, p < 0.0001, two-way ANOVA) (Figure 5E). This effect concerned the two main layers projecting to the striatum: layer 5 increased by 62% (p < 0.001) and layer 2/3 increased by 153% (p < 0.05) after late training. The density of CTB-A_{488}^+ cells in layer 2/3 somatosensory cortex was 631 ± 173 in naive, 1,194 ± 144 in early-trained, and 1,596 ± 224 in late-trained mice, and in layer 5 it was 2,850 ± 260 in naive, 3,237 ± 361 in early-trained, and 4,578 ± 506 in late-trained mice. In comparison, layer 6 projections remained unchanged, which is consistent with the fact that this layer targets mainly the thalamus (Thomson, 2010).

To go deeper into these anatomical rearrangements, we hypothesized that the increased density of pre-synaptic cortical cells after late training would be due to a denser axonal arborization of cortical terminals. To test this, we injected an AAV-CaMKII-GFP into the somatosensory cortex and quantified the axonal density of labeled corticostriatal cells in the striatum (Figures 5F and 5G). We observed a significant difference in the density of axonal segments in the striatum after late training (p = 0.0071). The axonal density was 61.5 ± 7.5 in naive (n = 6 mice) and 103.1 ± 11.2 in late-trained (n = 5 mice) mice (Figure 5H). In addition, the total length of the axonal segments was also significantly higher after training (p = 0.0179; total length in naive, 422 ± 57 μm, and in late, 690 ± 65 μm) (Figure 5H).

These results demonstrated that the dynamic reorganization of the DLS after late training is supported by anatomical rearrangements of inputs from somatosensory cortex.

Striatal HA cells are necessary for acquisition and maintenance of motor learning

Because HA cells strongly correlate with individual learning performance, we investigated whether they were directly responsible for motor skill acquisition and retention. We used a cFos-TRAP strategy (DeNardo and Luo, 2017; Giannotti et al., 2019; Josselyn et al., 2015; Tonegawa et al., 2018) to restrict the expression of hM4Di (silencing DREADD system) selectively in task-activated cells, to test whether silencing HA cells affects motor skill learning. We performed control experiments to confirm that HA cells were indeed cFos-positive cells, i.e., that they express the immediate-early gene related to high activity in neurons. First, cFos expression was efficiently induced by training, since we found a significant increase in the density of $cFos^+$ cells in DMS after early training and in DLS after late training with no expression in naive or running mice (Figure S5). The cFos expression was not dependent on the type of SPN (43 ± 4% of D1 SPNs in DMS and 55 ± 6% in DLS) (Figure S5), showing no apparent selectivity in direct or indirect pathway involvement. We next tested whether cFos-expressing cells were matching the HA cells. We used the cFos-TRAP strategy by co-injecting an AAV-cFos-ERT2-Cre-ERT2-PEST together with an AAV-DIO-mCherry reporter. Cre-recombinase was activated by 4-OH-tamoxifen (4-OHT) injection immediately after the training session, leading to a reliable expression of mCherry in cFos-expressing cells after 2 weeks (Figure S6). By co-injecting AAV-GCaMP6f with AAV-cFos-ERT2-Cre-ERT2-PEST and AAV-DIO-mCherry, we visualized both calcium-identified HA cells and cFos-expressing cells (Figure S7). The density of $cFos\text{-}mCherry^+$ cells was similar to the density of calcium-identified HA cells in both territories (p = 0.6538 for DMS and p = 0.6623 for DLS), and the overlap between HA cells and $cFos^+$ cells was high, in both DMS (78.9% ± 10.0%) and DLS (72.0% ± 8.8%) (Figure S7). Therefore, the cFos-TRAP strategy was suitable for selectively targeting and manipulating HA cells.

We used the DREADD system coupled to the cFos-TRAP strategy to selectively silence DMS or DLS HA cells. Mice were injected with AAV-cFos-ERT2-Cre-ERT2-PEST and either AAV-DIO-mCherry or AAV-DIO-hM4Di-mCherry and trained to the rotarod (Figure 6). Expression of either mCherry or hM4Di-mCherry was allowed by 4-OHT injection at the end of the training (Figures 6 and S6). On test day, mice were injected with clozapine-N-oxide (CNO) to activate hM4Di and silence HA cells prior to testing on the rotarod.

For the investigation of DMS, mice were first trained for 1 day (day 1) prior to the induction of mCherry or hM4Di-mCherry expression (Figure 6B) and were tested on day 15 (test day) (Figure 6C). On day 1, mCherry and hM4Di groups displayed similar performances (paired t(7) = 5.741, p = 0.0007, for mCherry and paired t(7) = 3.404, p = 0.0114, for hM4Di) and LIs (t(14) = 0.055, p = 0.9571), showing that the transfection *per se* had no effect (Figure 6B). On test day, the mCherry group significantly increased in performance between first and last trials (paired

(D and H) Representative EPSPs and representative curves of input/output sub-threshold response in response to a single stimulation, with increasing stimulation intensity. Bottom: bar graph of paired EPSP amplitudes for HA and LA cells with the same intensity of stimulation. DMS showed higher amplitudes in HA cells; DLS showed no significant difference.

(E and I) Representative 20 Hz trains of EPSPs and summations of EPSPs in SPNs after 20 Hz cortical electrical stimulation. Summary of the temporal summation, ratio of the fourth EPSP compared with the first EPSP for the different frequencies. In DMS, significant summation for LA cells (at 20 Hz) and none for HA cells, for all tested frequencies. In DLS, significant summation in both HA and LA cells with no significant difference, for all tested frequencies. Connecting lines in (C), (D), (G), and (H) illustrate the recorded pairs of HA/LA cells, but unpaired statistical tests were performed as HA and LA cells are independent. *p < 0.05, **p < 0.01. Data on bar graphs correspond to mean ± SEM and whisker-box plots to the median and 25th–75th percentiles (with min to max values).

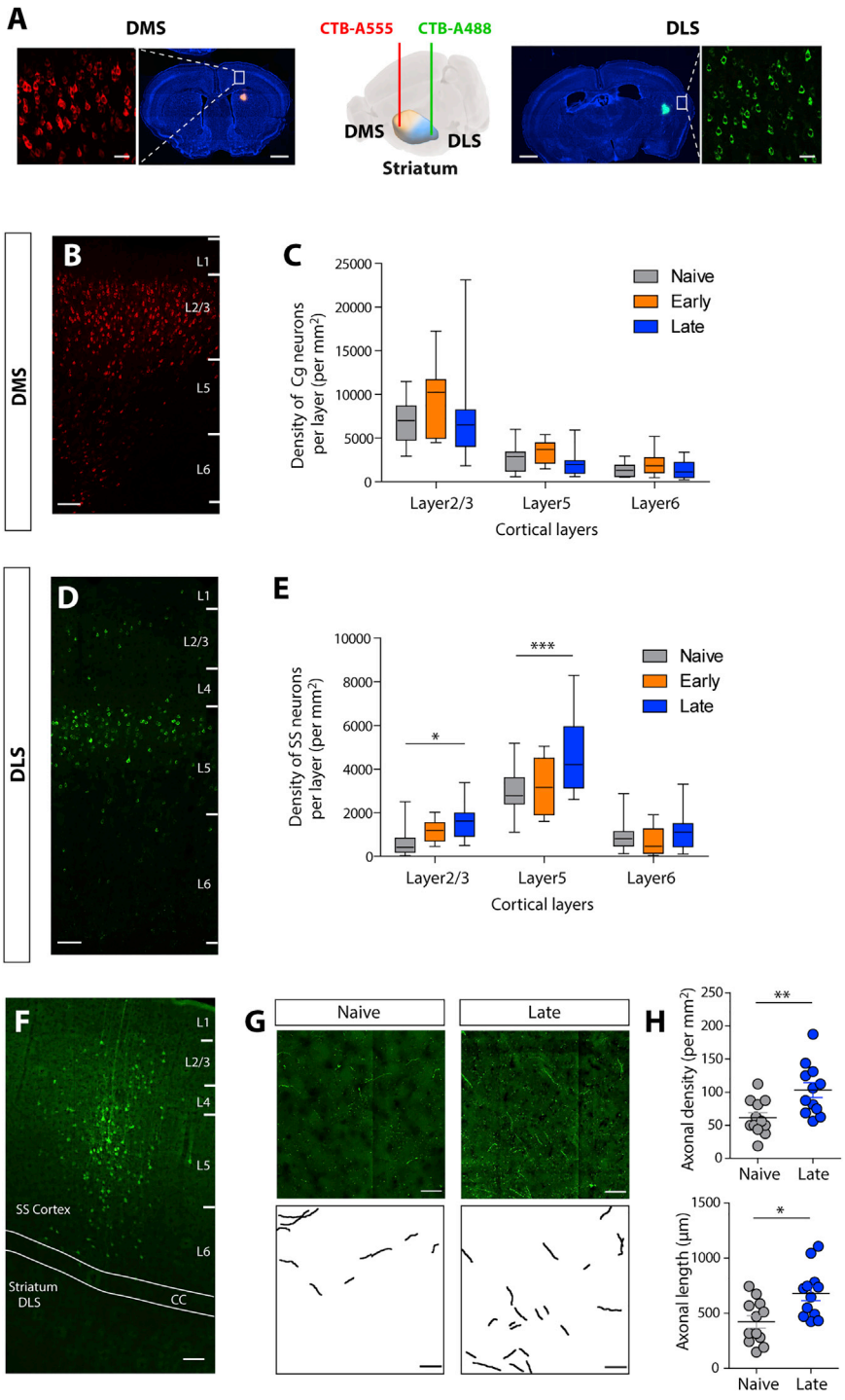

Figure 5. Motor learning induces anatomical plasticity of corticostriatal projections to DLS

(A) Middle: cholera toxin B (CTB) injections in the striatum. CTB-A_{555} was injected into the DMS and CTB-A_{488} into the DLS. Left and right: wide-field representative images of the injection sites, with DAPI labeling in blue (scale bars: 1 mm). Insets: confocal images of CTB-A_{555}-labeled layer 2/3 pyramidal neurons in cingulate cortex and CTB-A_{488}-labeled layer 5 pyramidal neurons in somatosensory cortex (scale bars: 20 μm).

(B and D) Cortical layer distribution of cingulate cortex labeled with CTB-A_{555} (B) and somatosensory cortex labeled with CTB-A_{488} (D) (scale bars: 100 μm).

(C) Quantification of the CTB-A_{555}^+ neurons: averaged number of cortical cells/mm^2 in the different layers for naive (n = 4 mice), early- (n = 5 mice), or late- (n = 5 mice) trained animals, on three slices (200 μm apart) per animal. No significant difference in the number of cortical CTB-A_{555}^+ cells in the different training conditions was found.

(E) Quantification of the number of CTB-A_{488}^+ neurons in naive (n = 5 mice), early- (n = 4 mice), or late- (n = 4 mice) trained animals. A significant increase in the somatosensory neuronal density after late training in layer 2/3 and layer 5 was seen. There was no effect of training on layer 6 projections; layer 4 is not presented, as the number of labeled cells was negligible.

(F) Confocal image of a representative injection site of AAV-CaMKII-GFP in the somatosensory cortex (SS cortex). The axons were measured in the striatum in DLS (scale bar: 100 μm).

(G) Representative confocal images of cortical axons in striatum in naive (left) or late-trained (right) animals and the corresponding traced and quantified axonal segments (scale bar: 50 μm).

(H) Quantification of axonal density (number of axonal segments/mm^2) and axonal length in striatum, in naive (n = 6 mice) and late-trained (n = 5 mice) animals. There are significantly higher number of axonal segments and higher total length of axonal segments after training. *p < 0.05, **p < 0.01, ***p < 0.001. Data on whisker-box plots correspond to the median and 25th–75th percentiles (with min to max values) and to mean ± SEM on the graphs.

t(7) = 6.893, p = 0.0002). In contrast, the hM4Di group had no improvement (paired t(7) = 1.200, p = 0.2696), with a significantly lower LI compared with control mice (t(14) = 2.231, p = 0.0168) (Figure 6C). Importantly, silencing random sub-sets of DMS SPNs during early training did not affect the performance (Figure S8). We next assessed whether silencing DMS HA cells could also affect late training. We repeated the experiments in mice trained for 7 days and tested their performance on day 21 (test day) (Figures 6D and 6E). Although the hM4Di group did not display significant improvement (paired t(7) = 0.7675, p = 0.4679), in contrast to the mCherry group (paired t(7) = 2.395, p = 0.0478), both groups had similar LIs (t(14) = 1.29, p = 0.2175) (Figure 6E). Together, these results show that DMS HA cells have a central role in the early phase, but it is not as important during the late phase of motor skill learning.

We used the same strategy for investigating the behavioral effect of DLS HA cell silencing (Figures 6F–6J). For the early-

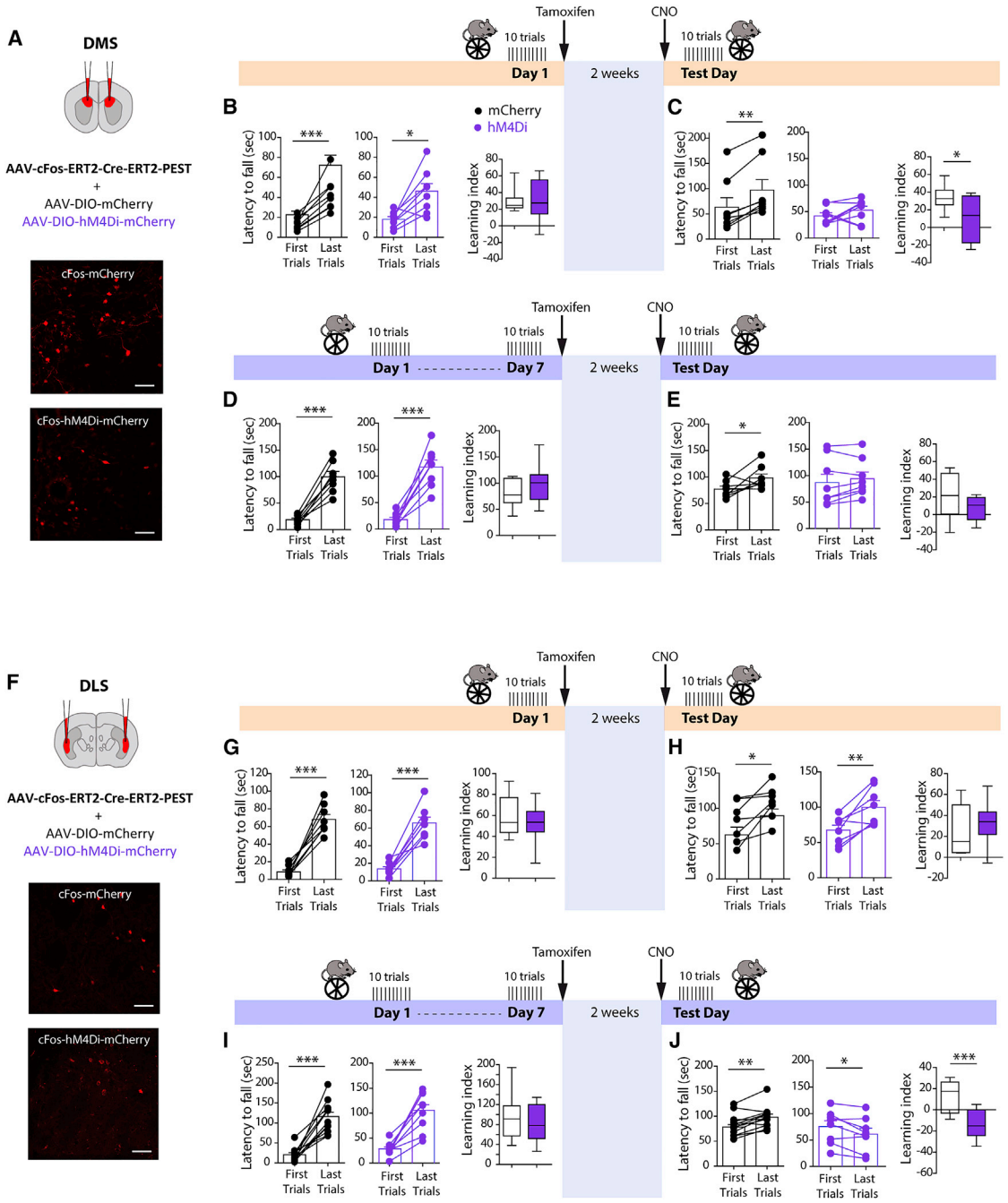

Figure 6. Silencing HA cells impairs performance

(A and F) Animals were injected in the DMS (A) or DLS (F) with AAV-cfos-ERT2-Cre-ERT2-PEST and AAV-DIO-mCherry for controls or AAV-DIO-hM4Di-mCherry for chemogenetic experiments. Confocal images of SPNs expressing mCherry or hM4Di-mCherry are shown (scale bars: 50 μm).

(B and C) Behavioral protocol for early training. Tamoxifen was injected at the end of early training (day 1); and 2 weeks later CNO was injected at the beginning of the test day. Performance of the animals on day 1 (B) and test day (C) for mCherry (black, n = 8 mice) and hM4Di (purple, n = 8 mice) groups. Paired latency to fall for each mouse for first and last trials, before (B) and after (C) induction of mCherry or hM4Di expression in DMS, is shown. Day 1: significant improvement in the performance for both groups and similar LI. Test day: the mCherry group still improved performance, but the hM4Di group did not and had a significantly lower LI.

(D and E) Behavioral protocol for late training. Tamoxifen was injected after late training on day 7 and CNO was injected at the beginning of the test day. Performance of the mice for day 1 to day 7 (D) and test day (E) for mCherry (black, n = 8 mice) and hM4Di (purple, n = 8 mice) groups. For days 1–7, significant improvement was seen in the performance between first trials and last trials for both groups, with similar LI. On test day, the mCherry group increased their performance and the hM4Di group showed no significant difference. LI was similar for both groups.

(legend continued on next page)

trained mice, the performance and LI of control and hM4Di mice was not affected at test day ($t(14) = 0.42$, $p = 0.6803$) (Figure 6H), suggesting that DLS HA cells were not involved in the early phase of learning. We next tested the impact of silencing DLS HA cells on late training. During the first week of training, both mCherry and hM4Di groups displayed a significantly increased performance between first and last trials (paired $t(10) = 7.09$, $p < 0.0001$, for mCherry and $t(7) = 5.943$, $p = 0.0006$, for hM4Di group) and similar LIs ($t(18) = 0.81$, $p = 0.4304$) (Figure 6I). On test day, the mCherry group still displayed a significant increase in performance (paired $t(10) = 3.39$, $p = 0.0068$) (Figure 6J). In contrast, the hM4Di group had strong impairments in their performance, marked by a significant decrease (paired $t(7) = 2.88$, $p = 0.024$) and a negative LI compared with the control group ($t(18) = 4.11$, $p = 0.0007$) (Figure 6J). Importantly, the silencing of random sub-sets of DLS SPNs during late training had no significant effect on the learning, thus confirming the selective role of HA cells for late training (Figure S8). These results demonstrate that DLS HA cells are necessary in the late stage of training.

DISCUSSION

We described here spatiotemporal reorganizations revealing striatal neuronal populations associated with specific phases of motor skill learning. Early training led to the appearance of sparse HA cells in the DMS and the start of a spatial restriction of the striatal cells recruited in the DLS. After late training, DMS activity returned to a basal-like state, while in DLS, HA cells became more spatially restricted. These two phases of network reorganization arose from distinct levels of plasticity: (1) reinforcement of synaptic connections from cingulate cortex onto DMS HA cells and (2) long-lasting anatomical rearrangements of somatosensory projections in the DLS. Importantly, targeted silencing of DMS and DLS HA cells impaired performance at different learning stages and highlighted that DMS early HA cells might be necessary for motor learning acquisition, and DLS HA clusters allowed for long-term retention of the motor skill.

Sequential involvement of DMS and DLS network reorganization during motor learning?

The striatum plays a crucial role during the different phases of learning, and many studies have described a preferential implication of DMS in the early phase and DLS in the late phase using lesions, global recordings, or transcriptional analysis (Bureau et al., 2010; Costa et al., 2004; Gremel and Costa, 2013; Matamales et al., 2020; Packard and McGaugh, 1996; Thorn et al., 2010; Wachter et al., 2009; Yin and Knowlton, 2006; Yin et al., 2004, 2006, 2009). Our results show post-training modifications of DMS networks mainly during the early phase and more pronounced modifications in DLS at the end of the training. In addition, silencing of HA SPNs seems to have a pronounced effect in the early phase for DMS and late phase for DLS. Nevertheless, our data also show learning-induced network reorganization in DMS during the late phase and in DLS during the early one. In DMS, even though the network seems to return to a naive level after late training, we observed that all network properties were not identical, for example, the synchronization of calcium responses. This highlights a long-lasting change in the DMS dynamics. In DLS the network reorganization was initiated already in the early phase, albeit with slighter modifications and no performance correlation, suggesting a gradual increase in its participation with extensive training. Recent reports have also described changes in neuronal activity patterns occurring simultaneously in the associative and sensorimotor striatum during both learning phases (Bergstrom et al., 2018; Kupferschmidt et al., 2017) and that intermingled activity of DMS and DLS during learning is even stronger after extensive training (Vandaele et al., 2019). Thus, the scheme may not be so binary and it should be regarded as more of a dynamic process by which decline in DMS activity precedes but overlaps with a gradual increase in DLS activity. Both striatal regions could thus be engaged long after initial acquisition, when skilled performance is consolidated.

Dynamic network reorganization in DMS and DLS

Rotarod training induced a transient decrease in the DMS response to cortical stimulation after early training. This is in apparent contradiction with previous recordings in DMS showing an increase in activity (Nonomura et al., 2018; Thorn et al., 2010; Yin et al., 2009), but recent publications have also highlighted an inhibition in DMS during the early phase of operant conditioning, particularly during lever-press sequences (Vandaele et al., 2019) and discrimination (Stubbendorff et al., 2019) tasks. Even though this could be interpreted as a disengagement of DMS, global inhibition could be a mechanism to reveal HA cells and increase the signal-to-noise ratio in the corticostriatal DMS network. In both striatal circuits, HA cells responded similarly regardless of the frequency of cortical stimulation and with higher correlated activity. This suggests that the reorganization revealed HA cells, which increase the signal-to-noise ratio and contribute to a better transmission of information, even for weaker cortical inputs. In DLS, no change, neither in the mean amplitude of the response nor in the global percentage of HA cells, occurred but a spatial reorganization leading to a progressive formation of clustered HA activity. While this clustering of activity in DLS was not observed after instrumental habitual behavior (O'Hare et al., 2016), other studies did report the formation of functional clusters in DLS, which activity was related to specific action, locomotion, or movement-related events (Barbera et al., 2016; Klaus et al., 2017; Parker et al., 2018). Further experiments should address if local striatal modulations of the SPN activity are at play during training. Learning may trigger

(G and H) For DLS-injected early-trained groups, performance on day 1 (G) and test day (H) for mCherry (black, n = 7 mice) and hM4Di (purple, n = 8 mice). On both day 1 and test day, both groups improved in performance, with similar LIs.
(I and J) Performance of the DLS-injected late-trained animals for day 1 to day 7 (I) and test day (J) for mCherry (black, n = 11 mice) and hM4Di (purple, n = 8 mice). (I) Significant improvement in performance between day 1 and day 7 for both groups, with similar LIs. (J) On test day, the mCherry group increased significantly in performance and hM4Di displayed a significant decrease in performance. LI was significantly lower for the hM4Di group ($p < 0.0001$, t test). *$p < 0.05$, **$p < 0.01$, ***$p < 0.001$. Data on whisker-box plots correspond to the median and 25th–75th percentiles (with min to max values).

modulation of local inhibitory interneurons, which could participate locally in the different reorganizations we observed in DMS and DLS. This would be in line with the role in instrumental learning of low-threshold spiking interneurons in DMS (Holly et al., 2019) and of fast-spiking interneurons (FSIs) in DLS (Martiros et al., 2018) and with a stronger response of FSIs than of SPNs to cortical primary somatosensory stimulation (Johansson and Silberberg, 2020; Lee et al., 2017).

It should be noted here that limitations of our *ex vivo* recordings are that we were stimulating only a sub-set of all the striatal cortical inputs and that we were probing network modifications after training. Thus the spatiotemporal network dynamics observed could be limited to the projections we stimulated *ex vivo*. However, cFos labeling, which is a proxy of *in vivo* activity during learning, revealed a high degree of overlap (75%) with HA cells. Since inhibiting these cells *in vivo* led to performance impairment, we can conclude that the spatiotemporal dynamics observed *ex vivo* are fundamental to the learning process and are a good indication of what happens *in vivo*.

Cortical inputs as important players in the reorganization

To explore the mechanisms, we focused here on the cortical inputs. Corticostriatal synaptic plasticity has been strongly associated with motor learning (Di Filippo et al., 2009; Koralek et al., 2012; Lerner and Kreitzer, 2011; Rothwell et al., 2015; Yin et al., 2009). Therefore, a first possible mechanism was that synaptic weight of cortical inputs could be specifically modified onto the HA cells. We validated this hypothesis for early DMS reorganization, coherent with a previous report of global potentiation of synaptic strength in the DMS (Yin et al., 2009) or enhanced *in vivo* synaptic activity from the frontal cortex after rotarod early training (Kupferschmidt et al., 2017). Interestingly, we describe here changes on HA cells only, and such modifications of synaptic weight could be coherent with the transitory state of the DMS HA cells during the early phase. We did not see any synaptic modifications in the DLS, while other studies reported long-lasting postsynaptic modifications after late training (Koralek et al., 2012; Rothwell et al., 2015; Yin et al., 2009). The differences with our findings may arise from the different experimental conditions used, such as the site of stimulation; in striatum, it is unspecific to all cortical afferents, as opposed to specific stimulations of the cingulate-DMS and sensorimotor-DLS pathways in our study. Also, in our experiments, we compared cortical connections to HA and LA cells within the same training condition, while in these studies the comparison was made between different training conditions.

Another hypothesis was that anatomical plasticity could account for the reorganization of corticostriatal networks. Axonal growth/modification has been suggested as a plausible mechanism for learning and memory formation (Chklovskii et al., 2004; Sampaio-Baptista et al., 2013; Zatorre et al., 2012). We saw an increase in the number of somatosensory cortical neurons projecting to DLS after motor learning. This was associated with an increased axonal density in the somatosensory-DLS pathway specifically after late training. The increased number of cortical cells would be caused by increased axonal sprouting rather than new axonal projections. We propose that the enhanced cortical connectivity is acting as a mechanism that reveals DLS HA cells after training. Nevertheless, our experiments do not allow us to distinguish whether the increased cortical connectivity was targeting more HA or LA cells. Procedural and motor skill learning was associated with axonal growth in other pathways (Scholz et al., 2015). Learning-induced axonal plasticity occurred as early as 11 days after a single-pellet reaching task training in areas adjacent to the motor cortex (Sampaio-Baptista et al., 2013) and after 5 days of associative motor learning in the adult cerebellum (Boele et al., 2013). Thus, these time scales are comparable to our observations of increased axonal projections after 7 days of training. Once formed, the motor skill is thought to be encoded within the sensorimotor loops, including the DLS; these long-lasting anatomical modifications could be responsible for the maintenance of the skill within striatal networks.

HA cells part of a subcortical motor memory trace?

The DMS and DLS HA cells were sparse, were activated by motor skill learning, and underwent either synaptic modifications or increased cortical inputs, respectively, and loss-of-function experiments demonstrated that they were necessary for proper memory retrieval. One could thus imagine that HA cells could be part of learning-related SPNs, similar to the engram cells described in hippocampus, amygdala, or cortex (Josselyn and Tonegawa, 2020; Rao-Ruiz et al., 2019). One original aspect is that the percentage of HA cells is negatively correlated with behavioral performance, showing that there is variability in size between animals correlated with performance. This could mean that learning leads to a decrease in the noise in the network with a limitation of the cells involved in motor learning. DMS and DLS HA cells would play different roles, since DMS HA cells appear only after early training and do not seem to be maintained after late training, indicating that they are important for the formation of the memory, but that the determinant long-term engram cells would be the clusters in DLS, as they are long-lasting.

The modulation of striatal activity has been correlated with many aspects of motor control and learning, such as locomotion, vigor, motivation, and movement in the selection of an action or concatenated actions (Gremel and Costa, 2013; Jin and Costa, 2010; Jurado-Parras et al., 2020; Klaus et al., 2017; Markowitz et al., 2018; Parker et al., 2018; Smith and Graybiel, 2013; Thorn et al., 2010). It will be important in the future to try to reconcile the different behavioral paradigms in motor learning and use their specificities to refine our understanding of the different components necessary to form a given skill.

Limitations of the study

Our aim here was to examine how motor learning was encoded and maintained within striatal population activity patterns during the different phases of learning. To answer this question, we probed corticostriatal activity *ex vivo* after training. This allowed the identification of populations of neurons that had undergone learning-induced plastic events and the study of how this affected the transmission of cortical information, which is critical for this type of learning. A limitation of this approach is that, on one hand, we remained unable to determine whether the

changes we observed in the dynamics occur during or after training and, on the other hand, since SPNs in the striatum are quiescent, we had to electrically stimulate the cortex to study their activity, removing the possibility of assessing the overall influence of natural stimuli in the spatiotemporal reorganization observed. These limitations could be overcome in the future by alternative approaches allowing recording throughout the learning process.

STAR★METHODS

Detailed methods are provided in the online version of this paper and include the following:

- KEY RESOURCES TABLE
- RESOURCE AVAILABILITY
  - Lead contact
  - Materials availability
  - Data and code availability
- EXPERIMENTAL MODELS AND SUBJECT DETAILS
  - Mice
- METHOD DETAILS
  - AAVs
  - Stereotaxic injections
  - Retrograde tracing studies
  - Axonal tracing studies
  - Behavioral training
  - Tamoxifen induced expression
  - *Ex vivo* two-photon imaging and multi-patch-clamp recordings
  - Immunohistochemistry
  - Drugs
- QUANTIFICATION AND STATISTICAL ANALYSIS
  - Behavior
  - Immunohistochemistry
  - CTB quantification
  - Axonal density quantification
  - Calcium imaging analysis
  - Electrophysiology
  - Statistical analysis

SUPPLEMENTAL INFORMATION

Supplemental information can be found online at https://doi.org/10.1016/j.celrep.2022.110623.

ACKNOWLEDGMENTS

The authors thank M. Albrieux, C. Kellendonk, M. Cazorla, A.S. Nicot, D. Robbe, and I. Bureau for careful reading of the manuscript and helpful comments. The authors would like to thank K. Deisseroth for making available the AAV-cFos-ERT2-Cre-ERT2-PEST-no WPRE virus, O. Manzoni and I. Bureau for sharing D1-tomato mice, S. Rotariu for help with open-field experiments, the Photonic Imaging Center, PIC-GIN facility (GIS-IBiSA ISdV, GIN), Y. Saoudi for help with image acquisitions, and the GIN animal facility for mouse care.

This work was supported by grants from Neuroglia (E.F.; supported G.Z. post-doctoral fellowship); the University of Grenoble Alpes Data Institute (N.T. and E.F.); Agence Nationale de la Recherche ANR-15-IDEX-02 NeuroCoG in the framework of the Investissements d'Avenir program (PhD fellowship for N.B.; E.F. and S.A.), ANR-19-CE37-0026-01 ProMeSS (E.F.), and ANR-18-CE16-0009-01 AXYON (F.S.); the Fondation pour la Recherche Médicale (FRM; DEI20151234418, F.S.); the Fondation pour la Recherche sur le Cerveau (FRC; F.S.); the Fondation Bettencourt Schueller (F.S.); and AGEMED program from INSERM (F.S.). The Saudou laboratory is a member of the Grenoble Center of Excellence in Neurodegeneration (GREEN).

AUTHOR CONTRIBUTIONS

E.F. conceived the project and E.F. and S.A. supervised the study; E.F., S.A., N.B., G.Z., and F.A. designed the experiments; N.B., G.Z., F.A., and E.F. performed the experiments; N.B., G.Z., F.A., G.B., N.T., and E.F. performed the analysis; N.T., F.S., S.A., and E.F. acquired the funding; N.B., G.Z., and E.F. wrote the manuscript; and all authors read and edited the manuscript.

DECLARATION OF INTERESTS

The authors declare no competing interests.

Received: August 26, 2021
Revised: January 21, 2022
Accepted: March 15, 2022
Published: April 5, 2022

REFERENCES

Barbera, G., Liang, B., Zhang, L., Gerfen, C.R., Culurciello, E., Chen, R., Li, Y., and Lin, D.T. (2016). Spatially compact neural clusters in the dorsal striatum encode locomotion relevant information. Neuron *92*, 202–213.

Becq, B., Badreddine, N., Tremblay, N., Appaix, F., Zalcman, G., Fino, E., and Achard, S. (2019). Classification of Types of Neurons from Calcium Imaging (XXVIIth Meeting of GRETSI), pp. 1–12.

Bergstrom, H.C., Lipkin, A.M., Lieberman, A.G., Pinard, C.R., Gunduz-Cinar, O., Brockway, E.T., Taylor, W.W., Nonaka, M., Bukalo, O., Wills, T.A., et al. (2018). Dorsolateral striatum engagement interferes with early discrimination learning. Cell Rep. *23*, 2264–2272.

Boele, H.J., Koekkoek, S.K., De Zeeuw, C.I., and Ruigrok, T.J. (2013). Axonal sprouting and formation of terminals in the adult cerebellum during associative motor learning. J. Neurosci. *33*, 17897–17907.

Buitrago, M.M., Schulz, J.B., Dichgans, J., and Luft, A.R. (2004). Short and long-term motor skill learning in an accelerated rotarod training paradigm. Neurobiol. Learn. Mem. *81*, 211–216.

Bureau, G., Carrier, M., Lebel, M., and Cyr, M. (2010). Intrastriatal inhibition of extracellular signal-regulated kinases impaired the consolidation phase of motor skill learning. Neurobiol. Learn. Mem. *94*, 107–115.

Cao, V.Y., Ye, Y., Mastwal, S., Ren, M., Coon, M., Liu, Q., Costa, R.M., and Wang, K.H. (2015). Motor learning consolidates arc-expressing neuronal ensembles in secondary motor cortex. Neuron *86*, 1385–1392.

Chklovskii, D.B., Mel, B.W., and Svoboda, K. (2004). Cortical rewiring and information storage. Nature *431*, 782–788.

Costa, R.M., Cohen, D., and Nicolelis, M.A. (2004). Differential corticostriatal plasticity during fast and slow motor skill learning in mice. Curr. Biol. *14*, 1124–1134.

Dayan, E., and Cohen, L.G. (2011). Neuroplasticity subserving motor skill learning. Neuron *72*, 443–454.

DeNardo, L., and Luo, L. (2017). Genetic strategies to access activated neurons. Curr. Opin. Neurobiol. *45*, 121–129.

Di Filippo, M., Picconi, B., Tantucci, M., Ghiglieri, V., Bagetta, V., Sgobio, C., Tozzi, A., Parnetti, L., and Calabresi, P. (2009). Short-term and long-term plasticity at corticostriatal synapses: implications for learning and memory. Behav. Brain Res. *199*, 108–118.

Doyon, J., Bellec, P., Amsel, R., Penhune, V., Monchi, O., Carrier, J., Lehericy, S., and Benali, H. (2009). Contributions of the basal ganglia and functionally related brain structures to motor learning. Behav. Brain Res. *199*, 61–75.

Durieux, P.F., Schiffmann, S.N., and de Kerchove d'Exaerde, A. (2012). Differential regulation of motor control and response to dopaminergic drugs by D1R and D2R neurons in distinct dorsal striatum subregions. EMBO J. *31*, 640–653.

Fino, E., Glowinski, J., and Venance, L. (2005). Bidirectional activity-dependent plasticity at corticostriatal synapses. J. Neurosci. *25*, 11279–11287.

Fino, E., Vandecasteele, M., Perez, S., Saudou, F., and Venance, L. (2018). Region-specific and state-dependent action of striatal GABAergic interneurons. Nat. Commun. *9*, 3339.

Fino, E., and Venance, L. (2011). Spike-timing dependent plasticity in striatal interneurons. Neuropharmacology *60*, 780–788.

Giannotti, G., Heinsbroek, J.A., Yue, A.J., Deisseroth, K., and Peters, J. (2019). Prefrontal cortex neuronal ensembles encoding fear drive fear expression during long-term memory retrieval. Sci. Rep. *9*, 10709.

Graybiel, A.M., and Grafton, S.T. (2015). The striatum: where skills and habits meet. Cold Spring Harb. Perspect. Biol. *7*, a021691.

Gremel, C.M., and Costa, R.M. (2013). Orbitofrontal and striatal circuits dynamically encode the shift between goal-directed and habitual actions. Nat. Commun. *4*, 2264.

Gruber, A.J., and McDonald, R.J. (2012). Context, emotion, and the strategic pursuit of goals: interactions among multiple brain systems controlling motivated behavior. Front. Behav. Neurosci. *6*, 50.

Hikosaka, O., Nakamura, K., Sakai, K., and Nakahara, H. (2002). Central mechanisms of motor skill learning. Curr. Opin. Neurobiol. *12*, 217–222.

Holly, E.N., Davatolhagh, M.F., Choi, K., Alabi, O.O., Vargas Cifuentes, L., and Fuccillo, M.V. (2019). Striatal low-threshold spiking interneurons regulate goal-directed learning. Neuron *103*, 92–101.e6.

Jin, X., and Costa, R.M. (2010). Start/stop signals emerge in nigrostriatal circuits during sequence learning. Nature *466*, 457–462.

Johansson, Y., and Silberberg, G. (2020). The functional organization of cortical and thalamic inputs onto five types of striatal neurons is determined by source and target cell identities. Cell Rep. *30*, 1178–1194.e3.

Josselyn, S.A., Kohler, S., and Frankland, P.W. (2015). Finding the engram. Nat. Rev. Neurosci. *16*, 521–534.

Josselyn, S.A., and Tonegawa, S. (2020). Memory engrams: recalling the past and imagining the future. Science *367*, eaaw4325.

Jurado-Parras, M.T., Safaie, M., Sarno, S., Louis, J., Karoutchi, C., Berret, B., and Robbe, D. (2020). The dorsal striatum energizes motor routines. Curr. Biol. *30*, 4362–4372.e6.

Klaus, A., Martins, G.J., Paixao, V.B., Zhou, P., Paninski, L., and Costa, R.M. (2017). The spatiotemporal organization of the striatum encodes action space. Neuron *96*, 949.

Koralek, A.C., Jin, X., Long, J.D., 2nd, Costa, R.M., and Carmena, J.M. (2012). Corticostriatal plasticity is necessary for learning intentional neuroprosthetic skills. Nature *483*, 331–335.

Kupferschmidt, D.A., Juczewski, K., Cui, G., Johnson, K.A., and Lovinger, D.M. (2017). Parallel, but dissociable, processing in discrete corticostriatal inputs encodes skill learning. Neuron *96*, 476–489.e475.

Lee, K., Holley, S.M., Shobe, J.L., Chong, N.C., Cepeda, C., Levine, M.S., and Masmanidis, S.C. (2017). Parvalbumin interneurons modulate striatal output and enhance performance during associative learning. Neuron *93*, 1451–1463.e1454.

Lerner, T.N., and Kreitzer, A.C. (2011). Neuromodulatory control of striatal plasticity and behavior. Curr. Opin. Neurobiol. *21*, 322–327.

Mandelbaum, G., Taranda, J., Haynes, T.M., Hochbaum, D.R., Huang, K.W., Hyun, M., Umadevi Venkataraju, K., Straub, C., Wang, W., Robertson, K., et al. (2019). Distinct cortical-thalamic-striatal circuits through the parafascicular nucleus. Neuron *102*, 636–652.e637.

Markowitz, J.E., Gillis, W.F., Beron, C.C., Neufeld, S.Q., Robertson, K., Bhagat, N.D., Peterson, R.E., Peterson, E., Hyun, M., Linderman, S.W., et al. (2018). The striatum organizes 3D behavior via moment-to-moment action selection. Cell *174*, 44–58.e17.

Martiros, N., Burgess, A.A., and Graybiel, A.M. (2018). Inversely active striatal projection neurons and interneurons selectively delimit useful behavioral sequences. Curr. Biol. *28*, 560–573.e565.

Matamales, M., McGovern, A.E., Mi, J.D., Mazzone, S.B., Balleine, B.W., and Bertran-Gonzalez, J. (2020). Local D2- to D1-neuron transmodulation updates goal-directed learning in the striatum. Science *367*, 549–555.

Melzer, S., Gil, M., Koser, D.E., Michael, M., Huang, K.W., and Monyer, H. (2017). Distinct corticostriatal GABAergic neurons modulate striatal output neurons and motor activity. Cell Rep. *19*, 1045–1055.

Nonomura, S., Nishizawa, K., Sakai, Y., Kawaguchi, Y., Kato, S., Uchigashima, M., Watanabe, M., Yamanaka, K., Enomoto, K., Chiken, S., et al. (2018). Monitoring and updating of action selection for goal-directed behavior through the striatal direct and indirect pathways. Neuron *99*, 1302–1314.e1305.

O'Hare, J.K., Ade, K.K., Sukharnikova, T., Van Hooser, S.D., Palmeri, M.L., Yin, H.H., and Calakos, N. (2016). Pathway-specific striatal substrates for habitual behavior. Neuron *89*, 472–479.

Packard, M.G., and McGaugh, J.L. (1996). Inactivation of hippocampus or caudate nucleus with lidocaine differentially affects expression of place and response learning. Neurobiol. Learn. Mem. *65*, 65–72.

Parker, J.G., Marshall, J.D., Ahanonu, B., Wu, Y.W., Kim, T.H., Grewe, B.F., Zhang, Y., Li, J.Z., Ding, J.B., Ehlers, M.D., et al. (2018). Diametric neural ensemble dynamics in parkinsonian and dyskinetic states. Nature *557*, 177–182.

Rao-Ruiz, P., Yu, J., Kushner, S.A., and Josselyn, S.A. (2019). Neuronal competition: microcircuit mechanisms define the sparsity of the engram. Curr. Opin. Neurobiol. *54*, 163–170.

Redgrave, P., Vautrelle, N., and Reynolds, J.N. (2011). Functional properties of the basal ganglia's re-entrant loop architecture: selection and reinforcement. Neuroscience *198*, 138–151.

Rothwell, P.E., Hayton, S.J., Sun, G.L., Fuccillo, M.V., Lim, B.K., and Malenka, R.C. (2015). Input- and output-specific regulation of serial order performance by corticostriatal circuits. Neuron *88*, 345–356.

Sampaio-Baptista, C., Khrapitchev, A.A., Foxley, S., Schlagheck, T., Scholz, J., Jbabdi, S., DeLuca, G.C., Miller, K.L., Taylor, A., Thomas, N., et al. (2013). Motor skill learning induces changes in white matter microstructure and myelination. J. Neurosci. *33*, 19499–19503.

Scholz, Jan, Niibori, Yosuke, Paul, W Frankland, and Jason, P Lerch (2015). Rotarod training in mice is associated with changes in brain structure observable with multimodal MRI. NeuroImage *107*, 182–189. https://doi.org/10.1016/j.neuroimage.2014.12.003.

Smith, K.S., and Graybiel, A.M. (2013). A dual operator view of habitual behavior reflecting cortical and striatal dynamics. Neuron *79*, 361–374.

Stubbendorff, C., Molano-Mazon, M., Young, A.M.J., and Gerdjikov, T.V. (2019). Synchronization in the prefrontal-striatal circuit tracks behavioural choice in a go-no-go task in rats. Eur. J. Neurosci. *49*, 701–711.

Thomson, A.M. (2010). Neocortical layer 6, a review. Front. Neuroanat. *4*, 13.

Thorn, C.A., Atallah, H., Howe, M., and Graybiel, A.M. (2010). Differential dynamics of activity changes in dorsolateral and dorsomedial striatal loops during learning. Neuron *66*, 781–795.

Tonegawa, S., Morrissey, M.D., and Kitamura, T. (2018). The role of engram cells in the systems consolidation of memory. Nat. Rev. Neurosci. *19*, 485–498.

Vandaele, Y., Mahajan, N.R., Ottenheimer, D.J., Richard, J.M., Mysore, S.P., and Janak, P.H. (2019). Distinct recruitment of dorsomedial and dorsolateral striatum erodes with extended training. Elife *8*.

Wachter, T., Lungu, O.V., Liu, T., Willingham, D.T., and Ashe, J. (2009). Differential effect of reward and punishment on procedural learning. J. Neurosci. *29*, 436–443.

Yin, H.H., and Knowlton, B.J. (2006). The role of the basal ganglia in habit formation. Nat. Rev. Neurosci. *7*, 464–476.

Yin, H.H., Knowlton, B.J., and Balleine, B.W. (2004). Lesions of dorsolateral striatum preserve outcome expectancy but disrupt habit formation in instrumental learning. Eur. J. Neurosci. *19*, 181–189.

Yin, H.H., Knowlton, B.J., and Balleine, B.W. (2006). Inactivation of dorsolateral striatum enhances sensitivity to changes in the action-outcome contingency in instrumental conditioning. Behav. Brain Res. *166*, 189–196.

Yin, H.H., Mulcare, S.P., Hilario, M.R., Clouse, E., Holloway, T., Davis, M.I., Hansson, A.C., Lovinger, D.M., and Costa, R.M. (2009). Dynamic reorganization of striatal circuits during the acquisition and consolidation of a skill. Nat. Neurosci. *12*, 333–341.

Zatorre, R.J., Fields, R.D., and Johansen-Berg, H. (2012). Plasticity in gray and white: neuroimaging changes in brain structure during learning. Nat. Neurosci. *15*, 528–536.

STAR★METHODS

KEY RESOURCES TABLE

REAGENT or RESOURCE	SOURCE	IDENTIFIER
Antibodies		
Primary antibody Anti c-Fos	Synaptic Systems	#226003; RRID:AB_2231974
Secondary antibody AlexaFluor 488 anti-rabbit	Invitrogen	A110085
Experimental models: Organisms/strains		
Mouse : C57BL/6J	Charles River	N/A
Virus strains		
AAV5-syn-GCaMP6f-WPRE-SV40	Addgene MA, USA	100837-AAV5
AAV8-cFos-ERT2-Cre-ERT2-PEST-no WPRE	Stanford Gene Vector and Virus Core, CA, USA	N/A
AAV5-hSyn-Cre	Addgene MA, USA	105553-AAV5
AAV5-hSyn-DIO-hM4D(Gi)-mCherry	Addgene MA, USA	44262-AAV5
AAV5-hSyn-DIO-mCherry	Addgene MA, USA	114472-AAV5
AAV1-CaMKII-GFP	Addgene MA, USA	105541-AAV1
Chemicals, peptides and recombinant proteins		
Isoflurane	Axience	N/A
4-Hydroxytamoxifen	Sigma Aldrich	H7904
Clozapine-N-oxide	Bio-Techne SAS	4936/50
Cholera Toxin Subunit B (Recombinant), Alexa Fluor™ 488 Conjugate	Thermo-Fisher	C34775
Cholera Toxin Subunit B (Recombinant), Alexa Fluor™ 555 Conjugate	Thermo-Fisher	C34776
Dimethylsulfoxide (DMSO)	Sigma Aldrich	D8418
Dako fluorescent mounting medium	Agilent	S302380-2
Software and algorithms		
R3.5.2	r-project	https://www.r-project.org/
Code and dataset for calcium analysis	This paper	https://zenodo.org/record/6331931
FIJI	Fiji software	https://fiji.sc/
Fitmaster	HEKA	https://www.heka.com/
GraphPad Prism	GraphPad Software	https://www.graphpad.com/
Imspector	LaVision BioTec	https://www.miltenyibiotec.com/
Patchmaster v2x32	HEKA Elektronik	https://www.heka.com/

RESOURCE AVAILABILITY

Lead contact

Further information and requests for resources and data supporting the findings of this study are available upon reasonable request. All requests should be directed to and will be fulfilled by the Lead Contact, Elodie Fino (elodie.fino@inserm.fr).

Materials availability

This study did not generate new unique reagents.

Data and code availability

An example of a dataset is available at Zenodo and is publicly available with the code at the DOI listed in the key resources table. All original code has been deposited at Zenodo and is publicly available as of March 6th 2022. The DOI is listed in the key resources table.

Any additional information required to reanalyze the data reported in this paper is available from the lead contact upon request.

EXPERIMENTAL MODELS AND SUBJECT DETAILS

Mice

C57BL6 mice (*Mus musculus*) of 1.5 to 4 month-old and Drd1-TdTomato mice of both sexes were used and housed in temperature-controlled rooms with standard 12 hours light/dark cycles and food and water were available *ad libitum*. Every precaution was taken to minimize stress and the number of animals used in each series of experiments. All experiments were performed in accordance with EU guidelines (directive 86/609/EEC) and in accordance with French national institutional animal care guidelines (protocols #8241 and #29200).

METHOD DETAILS

AAVs

Adeno-associated viruses (AAVs of serotype 1, 5 and 8) were used to express different genes in striatal cells. AAV5-syn-GCaMP6f-WPRE-SV40 was purchased from UPennCore (PA, USA), the AAV8-cFos-ERT2-Cre-ERT2-PEST-no WPRE from Stanford Gene Vector and Virus Core (CA, USA) and AAV5-hSyn-Cre, AAV5-hSyn-DIO-hM4D(Gi)-mCherry, AAV5-hSyn-DIO-mCherry or AAV1-CaMKII-eGFP were purchased from Addgene (MA, USA).

Stereotaxic injections

Stereotaxic intracranial injections were used to deliver AAVs or CTB (Cholera Toxin B) in striatum. Mice were anesthetized with 2.5 % isoflurane and placed in a stereotaxic frame (Kopf). Under aseptic conditions, the skull was exposed and leveled and a craniotomy was made with an electric drill. The viruses ($\approx 10^{12}$ genomic copies per mL) were injected through a pulled glass pipette (pulled with a P-97 model Sutter Instrument Co. pipette puller) using a nanoinjector (World Precision Instruments, Germany). The pulled glass micropipette was slowly lowered into the brain and left 1 min in place before starting the injection of the virus at an injection rate of 100 nL per min. A volume of 400 nL of the viruses was enough to infect a large proportion of DMS or DLS. The injections targeted the DMS at coordinates AP + 1.1mm, ML 1.2, DV - 1.9 and the DLS at AP - 0.3, ML 2.3, DV - 2.45. Following injections, we waited 5 min before raising the pipette out of the brain. To minimize dehydration during surgery mice received a subcutaneous injection of 1mL of sterile saline. Postoperatively mice were monitored on a heating pad for 1 h before being returned to their home cage. Mice were then monitored daily for 4-5 days. Behavioural and/or imaging experiments started 15 to 20 days after injection, a period sufficient to allow for a good expression of AAVs. We observed similar expression of GCaMP6f in all striatal neurons in DMS or DLS in injected mice with viral vectors.

Retrograde tracing studies

Retrograde tracer Cholera toxin subunit (CTB) pre-labelled with an Alexa-488 (CTB-488) or Alexa-555 fluorophore (CTB-555) (0.25 μg/μl dissolved in saline; Thermo-Fisher Scientific) was used to retrogradely label cortical neurons projecting to DMS or DLS. In order to study learning-induced changes in the density of cortical neurons projecting to each striatal territory, mice were injected in the left hemisphere with 400 nL of CTB-A_{555} in DMS and 400 nL of CTB-A_{488} in DLS in naive animals or one day after early or late training. 5 days after stereotaxic injections mice were perfused transcardially with PFA 4 % and brains were removed and sliced as described in the immunohistochemistry section. Fifty micrometers coronal slices were obtained using a cryostat (Microm HM 560, ThermoScientific). Coronal sections spanning the whole striatum (1.70 mm to -2.18 mm AP from Bregma, according to Paxinos Atlas) were incubated for 2 h with 1:4000 DAPI, then rinsed 3 times in PBS and mounted with Dako fluorescent mounting medium (Agilent) on microscope slides.

Axonal tracing studies

AAV1-CaMKII-eGFP was injected the somatosensory cortex to label cortical neurons and to determine whether learning induced changes in the corticostriatal axonal density. The injection conditions were reproducible in targeting the somatosensory cortex, allowing us to compare the axonal density between the naïve and trained animals. The reproducibility of the injections is corroborated by the similar distributions for both groups (Figure 5H). Mice were injected with 300nL of virus, diluted to have sparse labelling. The injection targeted the left somatosensory cortex at coordinates: AP - 0.3, ML 3.7, DV - 1.6. Two weeks later, mice were either late-trained, or remained naïve. Mice were sacrificed at the end of training and brains were removed and sliced as described in the immunohistochemistry section. Fifty micrometers horizontal slices were incubated for 15min with 1:4000 DAPI, then rinsed 3 times in PBS and mounted with Dako fluorescent mounting medium (Agilent) on microscope slides.

Behavioral training

An accelerating rotarod was used as a motor skill learning paradigm (Panlab). In the days prior to the training, mice were acclimated to the room and to handling. For each trial the mouse was placed on the moving rod at the constant speed of 4 rpm. The rotation of the rod was then increasing from 4 to 40 rotations per min over 300 s (Kupferschmidt et al., 2017; Yin et al., 2009). Each trial ended when the mouse fell off the rod or when the 300 s had elapsed. There was a resting period of 300 s between trials. Animals were trained with 10 trials per day for either 1 day (early training) or 7 days (late training). This training protocol was previously described as a reliable test for motor skill learning or procedural learning (Buitrago et al., 2004; Costa et al., 2004; Kupferschmidt et al., 2017; Yin et al., 2009).

Tamoxifen induced expression

Mice were injected as previously described with AAV8-cFos-ERT2-Cre-ERT2-PEST and AAV-hSyn-DIO-mCherry or AAV5-hSyn-DIO-hM4D(Gi)-mCherry. Two weeks later, mice were trained on the accelerated rotarod (early or late training) and right after injected intraperitoneally with 4-Hydroxytamoxifen (4-OHT; Sigma-Aldrich) (50 mg/kg) to induce recombination. Expression of the floxed AAVs was allowed for 2 weeks and after this time mice were injected with Clozapine-N-Oxide (CNO, i.p., 3 mg/kg) 30 minutes before training. Brains were extracted 2 hours after training for histological characterization.

Ex vivo two-photon imaging and multi-patch-clamp recordings

Brain slice preparation

Two weeks after AAVs injections, and after rotarod training, brain slices preserving DMS and DLS with their cortical inputs coming from sensory and cingulate cortex respectively were prepared as previously described (Fino et al., 2005, 2018). Animals were anesthetized with isoflurane before extraction of the brains. We prepare brain slices (300 μm) using a vibrating blade microtome (VT1200S, Leica Microsystems, Nussloch, Germany). Brains were sliced in a 95 % CO_2 and 5 % O_2-bubbled, ice-cold cutting solution containing (in mM) 125 NaCl, 2.5 KCl, 25 glucose, 25 $NaHCO_3$, 1.25 NaH_2PO_4, 2 $CaCl_2$, 1 $MgCl_2$, 1 pyruvic acid, and then transferred into the same solution at 34°C for one hour and then moved to room temperature.

Two-photon calcium imaging

Genetically-encoded Ca^{2+} indicator GCaMP6f was used for calcium imaging of somas of striatal cells. GCaMP6f was expressed with recombinant AAVs injected in DMS or DLS. Two-photon calcium imaging was performed at 940 nm with a TRiMScope II system (LaVision BioTec, Germany) using a resonant scanner, equipped with a 20x/1.0 water-immersion objective (Zeiss) and coupled to a Ti:Sapphire laser (Chameleon Vision II, Coherent, > 3 W, 140 fs pulses, 80MHz repetition rate). The average power of the laser emitted was set at ∼40-50 mW on sample. Fluorescence was detected with a GaAsP detector (Hamamatsu H 7422-40). Scanning and image acquisitions were controlled with Imspector software (LaVision BioTec, Germany) (15.3 frames per second for 1024 x 1024 pixels, between 50 to 150 μm underneath the brain slice surface, with no digital zoom). Typical field of view for calcium imaging was 392 x 392 μm.

Cortical stimulation protocols

Electrical stimulations were applied with a bipolar electrode (MicroProbes, USA). For DMS recordings, stimulating electrode was placed in the layer 5 of cingulate cortex from para-sagittal slices, and for DLS recordings, it was placed in the layer 5 of somatosensory cortex from horizontal slices, as previously described (Fino et al., 2018). Electrical stimulations were monophasic at constant current (Iso-Flex, AMPI, Science Products). Single cortical stimulations or trains of stimulations were delivered; trains consist of 5 stimulations delivered at different frequencies (5, 10, 20, 50 Hz). Single or trains of stimulations were applied at 0.1 Hz, a frequency for which no short- or long-term changes are observed (Fino et al., 2005). Single stimulation duration ranged from 0.1 to 1 ms, for subthreshold and suprathreshold activity (for calcium imaging experiments). The results shown in Figures 1 and S1 were obtained at 20 Hz, as this frequency was eliciting a reliable response.

Electrophysiological recordings

Whole-cell patch-clamp recordings of SPNs were performed with borosilicate glass pipettes (5-8 MΩ) containing (mM): 127 K-gluconate, 13 KCl, 10 HEPES, 10 phosphocreatine, 4 ATP-Mg, 0.3 GTP-Na, 0.3 EGTA (adjusted to pH 7.35 with KOH). Slices were continuously superfused with the extracellular solution containing (mM): 125 NaCl, 2.5 KCl, 25 glucose, 25 $NaHCO_3$, 1.25 NaH_2PO_4, 2 $CaCl_2$, 1 $MgCl_2$, 10 μM pyruvic acid bubbled with 95 % O_2 and 5 % CO_2. Slices were visualized under a microscope (Slicescope Scientifica, London, UK) with a 5x/0.15 objective for the placement of the stimulating electrode and a 20x/1.0 water-immersion objective for localizing cells for whole-cell recordings. SPNs were distinguished from other striatal neurons such as interneurons based on morphology and/or passive and active membrane properties (Fino and Venance, 2011). Signals were amplified using EPC10-2 amplifiers (HEKA Elektronik, Lambrecht, Germany). Current-clamp recordings were filtered at 2.5 kHz and sampled at 5 kHz and voltage-clamp recordings are filtered at 5 kHz and sampled at 10 kHz using the program Patchmaster v2x32 (HEKA Elektronik). Recordings were performed at 32-35°C to maintain physiological temperature conditions.

Immunohistochemistry

Quantification of cFos expressing striatal cells was done by immunohistochemistry targeting cFos. Two hours after the end of the training, mice were deeply anaesthetized with Dolethal (2 mL/kg) injected intraperitoneally, then transcardially perfused with first phosphate buffered saline (PBS) and finally 4 % paraformaldehyde (AntigenFix, Diapath). Following perfusion, brains were postfixed in 4 % paraformaldehyde for 24 hours at 4°C. Brains were washed with PBS 1X and then incubated in a 30 % (wt/vol) sucrose solution at 4°C until they sank. Next, they were placed in a mold with OCT and kept at −80°C. Twenty-four hours before slicing, brains were placed at −20°C. Forty micrometers coronal slices were obtained using a cryostat (Microm HM 560, ThermoScientific). Slices were kept in a cryoprotective solution at −20°C. Coronal sections were blocked with PBST (PBS with 0.3 % Triton X-100) with 5 % (vol/vol) normal goat serum for 1 h 30 and then incubated with the first primary antibody at 4°C for 24 h (rabbit anti-c-Fos 1:500, Synaptic Systems #226003). The next day, slices underwent three 10 min wash steps in PBS, next they were incubated for 2 h with secondary antibodies (1:200 AlexaFluor 488 anti-rabbit, Invitrogen). Finally, slices underwent three more 10 min wash steps in PBS, followed by mounting and coverslipping with Dako fluorescent mounting medium (Agilent) on microscope slides.

Drugs

Clozapine-N-oxide (Bio-Techne SAS) was first dissolved in dimethylsulfoxide (DMSO, Sigma, final concentration 25 μg/μL), then aliquoted and stored at −20°C. For intraperitoneal injections, frozen aliquots were put at room temperature, and then further diluted in 0.9 % sterile saline solution to a final concentration of 0.3 μg/μL. The solution was delivered intraperitoneally (3 mg/kg) and, after the injection, the animals were placed back in the home cage for 30 min before the start of the experiment. 4-Hydroxytamoxifen (4-OHT) was dissolved by sonication for about 15 minutes (until total dissolution) in 10 % EtOH / 90 % corn oil at 40°C to get a final concentration of 5 mg/ml. Mice were injected with 50 mg/kg of 4-OHT (200 μL). 4-OHT was prepared on the same day of the experiment.

QUANTIFICATION AND STATISTICAL ANALYSIS

Behavior

The time to fall (latency) from the accelerating rotarod was recorded to measure the performance of the animals in the motor skill learning. In accordance with previous studies (Buitrago et al., 2004; Yin et al., 2009) trial 1 and 2 data are pooled as first trials and trial 9 and 10 data pooled as last trials for each day. We computed a learning index (LI) (Buitrago et al., 2004; Kupferschmidt et al., 2017) by subtracting first trials from last trials of Day1 for early training, and first trials of Day 1 and averaged trials of Day 7 for late training (last part of the plateau at the end of the training). The averaged values of the LI were calculated for all tested animals (in the different experimental sections) and were 35.1±5.6 for early training (n= 21 mice) and 48.9±6.3 for late training (n= 40 mice). Animals with LI equal or superior to these values were considered to have learned the task and used for further analysis.

Immunohistochemistry

Images were acquired using a confocal microscope (LSM710, Zeiss, Germany). Z-stacks (20-30 μm) with 2 μm step size were acquired in DMS or DLS with a 20x/0.8 objective. Concerning the cFos immunostainings, we quantified the density of cFos expressing neurons in 3 mice per condition. For each mouse, we acquired Z-stacks on 2-3 different coronal slices on the anteroposterior axis per territory (DMS and DLS) in one or two hemispheres. Each Z-stack was first filtered using a White Top Hat Morphological filter (MorphoLibJ plugin, FIJI software). Then, 3D object counter plugin was applied on the Z-stack obtained, with a Threshold set to 25 and a size filter set to 200 to remove low signal and small objects. Finally, one plane from the Z-stack was taken and 2 or 3 fields (400 x 400 μm) were used to determine the density of cells with high cFos expression. The quantification of mCherry+ and hM4Di-mCherry+ cells was done in fields of 400 x 400 μm to be compared with the number of HA cells we observed in DMS and DLS (Figures 1 and S6). We quantified the number of cells with automatized detection using FIJI software in 2-5 mice per condition (no tamoxifen, mCherry+ and hM4Di-mCherry+ for cFos-cre virus and mCherry+ and hM4Di-mCherry+ for hSyn-cre virus), in 2-3 different coronal slices on the anteroposterior axis and within 2-3 fields of 400 x 400 μm per slice.

CTB quantification

For the quantification of CTB-555+ cells in cingulate cortex (Cg - > DMS projections) and CTB-488+ cells in somatosensory cortex (Somatosensory - > DLS projections), 3 slices per region for each animal were imaged with a microscope slide scanner (Axio Scan.Z1, Zeiss, Germany) with a 20x /0.8 objective. The analysis was performed blindly to the training conditions. Analysis of the CTB-555+ cells in cingulate cortex was performed for slices spanning 1.2 mm to 0.2 mm AP from Bregma according to Paxinos Atlas, and for CTB-488+ cells in somatosensory cortex from -0.1 mm to -1.1 mm. Quantification of striatal projecting neurons was performed over all the cingulate and somatosensory cortex layers for each slice using the 'Cell Counter' plugin by Kurt De Vos (University of Sheffield, UK) (FIJI software). For cell counting, we only considered cells in which the soma was distinguishable for showing its nucleus labelled with DAPI. For each slice, cortical area was delimitated based on Paxinos Atlas, then we used DAPI staining to identify the layering in each cortical region. Density values per layer for each slice were obtained dividing the total number of neurons by the area of the cortical layer in which it was present. These density values per slice for each animal were normalized to the corresponding total area of the injection site (Figure S4). To obtain the total area of the injection site for each animal, all slices containing fluorescence from the injections were imaged with an inverted microscope (AxioObserver7 microscope, Zeiss, Germany) with a 5x /0.15 objective. Then for each slice a region of interest delineating the injection site was drawn and its area was measured using FIJI software. The total area of injection site was calculated as the sum of all the area measured/animal.

Axonal density quantification

Cortical axons were imaged in the striatum using a confocal microscope (LSM 800, Zeiss, Germany) with a 20x/0.8 objective. Z-stacks of 30μm with 0.5μm step size were taken for both naïve and late-trained conditions. First a standard deviation intensity projection was made on each stack. After enhancing local contrast (CLAHE in FIJI with a maximum slope = 3), one to three 400 x 400 μm ROIs were used in each field for analysis. The 'Neuroanatomy-SNT' plugin in FIJI was used to trace axonal segments to quantify their number and measure their length. Each visible axon was selected and counted. Quantification were done in 1-3 horizontal slices on the dorsoventral axis per animal and within 1-3 fields of 400 x 400 μm per slice.

Calcium imaging analysis

GCaMP6f fluorescence signals were analysed with custom-built procedures using R3.5.2 in RStudio environment. The analysis was performed blindly to the training condition and by different experimenters. Several semi-automatic algorithms have been developed for Region of interests (ROIs) identification but we found that they were not robust enough to identify all the neurons in the striatum. We thus manually selected ROIs based on morphology using FIJI software. Then we extracted mean grey values and (x, y) coordinates for each ROI/slice. Calcium recordings were 700-1000 frames long (around 1 min) and included 7-9 stimulations of cortical afferents (Figure S1). Let x(t) be the averaged intensity values of pixels in the ROI at time t for one cell. ΔF/F is obtained using y(t) = (x(t) - x0) / x0, where x0 is the mean value of the 50 % lowest values in the last 10 s. ΔF/F was then filtered with a Savitsky-Golay filter of order 3 on sliding windows of 7 frames (0.458 s). For each cell, the amplitude of response to cortical stimulations was calculated by averaging ΔF/F for 5 responses (stimulations #2 to #6). To this aim, fluorescence signals were extracted for each cell on windows of 40 frames (2.6 s) centered on the time of the first maximal amplitudes of ΔF/F (peaks) detected on cells after stimulus (Figures S1E and S1F). Within this time window, for each response, the start and the peak were detected. The amplitude of response was measured as a Delta between the values from the start and the peak points. A cell was defined as active if its amplitude of response was above a threshold defined as M+2SD, with mean (M) and standard deviation (SD) calculated individually for each neuron through the whole recordings; below this threshold, the cell was considered as inactive (Figures S1E and S1F). The color coded maps were extracted with the measure of each cell amplitude within the field of view and inactive cells are represented in white (Figures S1G and S1H). We distinguished responses from SPNs and other cell types of striatal neurones thanks to a cell-sorting method based on calcium responses we previously developed (Becq et al., 2019). We are thus confident that the majority of the cells analysed were SPNs.

To extract the highly active (HA) cells population, we used two different methods. First, to normalize the activity throughout the training conditions, we applied a thresholding analysis using the average of the response amplitude in naive animals as reference (calculated from all SPNs in Naïve animals for each frequency and each territory). The group containing the cells with the highest amplitude (superior to the threshold) was defined as the HA cells and represents X % of cells in the slice. Second, to explore whether clusters of activity (HA cells restricted in space) were observed in striatal networks after learning, we used a k-means analysis. This analysis considered both the amplitude of response and the x,y position of each cell within the field and each animal is considered independently. Cells were first sorted by their amplitude of response (HA cells) and then, by the inter-distances between the HA cells. In that case, k the optimal number of groups was defined using the 'elbow method', by visual inspection of the plot, of the function to compute total within-cluster sum of squares with k varying from 1 to 10 and determining the inflection point of the curve. There was no significant difference in k between training conditions. The group containing the cells with the highest amplitude was defined as the HA cells cluster and contains X % of cells in the slice. The cluster area was computed using the convex hull formed by the cluster HA cells. The cluster area percentage was obtained as the HA area relative to the total area of the field (area of the convex hull from the active cells at the edges of the field of view). Both analyses showed a change in amplitude in different training conditions and no spatial re-organization in DMS, while in DLS, there was no change in amplitude in the different groups but a strong spatial reorganization with the formation of clusters.

Pairwise correlations were computed using Pearson's correlation between signals extracted on windows of 40 frames (2.6 s) centered on the time of the first maximal amplitudes of ΔF/F (peaks) detected on cells after stimulus. Examples of correlation matrices for one slice, representing the pairwise correlations between cells in HA and LA cells are given in Figures S3E and S3F.

Electrophysiology

Electrophysiological properties of striatal neurons were quantified as follows. Input resistance (Ri) was measured by repeated current injections (-20 pA, 500 ms) and frequency was measured for current steps +30 pA above AP threshold. Whole cell recordings were not analyzed if the input resistance was varying more than 20 % throughout the recordings. Cortically-evoked single EPSP amplitude ranged from 1 mV to 30 mV. SPNs were held at their physiological membrane potential, in average -78.2±0.3 mV (n= 41) and there was no statistical difference in the holding membrane potentials between the different experimental conditions. We assessed short-term dynamics of cortically-evoked excitatory post-synaptic potentials (EPSPs) with trains of stimulation. We measured short-term temporal summation by measuring the total amplitude of each EPSP (from baseline to the peak of the response) and normalizing it to the amplitude of the first EPSP. In a subset of experiments combining different frequencies, the normalized amplitude corresponded to the ratio between the fourth EPSP of the train compared to the first one. We compared the effect for each EPSP of the train and the fourth one was chosen as a representative. Spiking probability was measured as the occurrence of a single action potential induced by a single cortical stimulation of the cerebral cortex. Spiking probability was measured at a stimulation intensity giving around 50 % spikes for the LA cells and the corresponding spiking probability for the same stimulation intensity for HA cells. We repeated 6 to 8 trials to calculate the averaged spiking probability. The latency to spike was the time between the electrical stimulation and the peak of the action potential. Data analysis was carried out in Fitmaster (HEKA Elektronik, Germany).

Statistical analysis

The data are presented and plotted as mean ± SEM (unless otherwise stated), where SEM refers to standard error of the mean. Data on whisker-box plots correspond to the median and 25th–75th percentiles (with min to max values).p values are represented

by symbols using the following code: * for $p< 0.05$, ** for $p< 0.01$, *** for $p< 0.001$. Exact p values and statistical tests are stated in the figure legends or in the core of the manuscript. Statistical analysis is performed using Prism 5.0 (GraphPad, San Diego, USA) or R environment. The sample size for the different sets of data is mentioned in the text or in the respective figure legends. Normality of each data set was checked using D'Agostino and Pearson's test. Statistical significance was assessed using Student's t-test or Mann-Whitney's U-test and Wilcoxon's signed rank test for unpaired and paired data, respectively. One-way Anova was used to compare all the effects together in DMS and DLS between the different training conditions. Pearson correlation was used for relationship between cluster size and learning index. Two-way Anova followed by Bonferroni *post-hoc* test was used to compare different parameters (calcium dynamics, anatomical modifications) evolving throughout the training conditions, electrophysiological I/O curves, short-term plasticity and learning curve in different treatment conditions.